UNIVERSITÀ DEGLI STUDI DI PADOVA

INDUSTRIAL ENGINEERING DEPARTMENT

MASTER'S DEGREE IN CHEMICAL ENGINEERING
FOR SUSTAINABLE DEVELOPMENT

Master's Degree Thesis in Chemical Engineering
for Sustainable Development

SOLID OXIDE FUEL CELLS MODELING UNDER STEADY-STATE AND FORCED OSCILLATIONS REGIMES

Supervisor: Prof. Paolo Canu

Student: NICOLA ZANETTI

ACADEMIC YEAR: 2016-2017

“The Universe is under no obligation

to make sense to you.”

Neil deGrasse Tyson

Abstract

This study is part of a collaboration between the department of Chemical Engineering and the department of Chemical Sciences at University of Padua. The goal is to develop new materials that can be used to manufacture solid oxide fuel cells operating at lower temperatures. In order to do this, the inherent properties of said materials, like electronic and ionic conductivities, or catalytic properties, are not enough, because a fuel cell is a complex system in which many phenomena happen at the same time. In order to optimize the performance, this study focused on the development of a mathematical model of the cell, which has been validated with literature data and that can be used to evaluate the influence that material properties, manufacturing specifications and operating conditions have on the involved phenomena and on overall efficiency.

This model uses a finite element simulation software, COMSOL Multiphysics, to represent the behavior of the cell. The output of the model has been validated with literature data without resorting to adjustable parameters, and can therefore be assumed to adequately represent the phenomena under consideration. The model has then been used to quantify the effect that changing several parameters has on the cell, both under steady-state conditions (analysis of the polarization curve, to evaluate overall performance) and with forced perturbations (electrochemical impedance spectroscopy, to discern the contributions that the various phenomena give to the performance).

Since the model has been validated without fitting adjustable parameters, it could be used in the future on cell prototypes using new materials to evaluate hard to obtain parameters like reaction kinetics, once other properties are known.

Ringraziamenti

Desidero innanzitutto ringraziare il prof. Paolo Canu per il supporto e la pazienza dimostratami: non credo molti avrebbero fatto lo stesso.
Ringraziamento speciale per gli amici di una vita, che avranno sempre un posto particolare nel mio cuore: in ordire rigorosamente alfabetico, Enrico, Max, Michele, Pit, Riccardo. Più di due decenni di amicizia, e ancora non vi siete stufati di me! Al gruppo ci aggiungo pure Dapo, conosciuto qualche anno dopo ma con cui ho condiviso buona parte della vita adulta.
Vorrei poter nominare tutte le altre persone che ho conosciuto negli anni e che hanno significato qualcosa per me, ma finirei lo spazio: raggruppandole in grosse categorie, tutta la gente su Simposium che non è già stata nominata sopra, i coinquilini che ho contribuito a far ingrassare notevolmente, i Salesians di Bologna, tutta la banda del vecchio Pollaio, i Performers (in particolar modo Tommy per le numerose serate a bere Jackhammer e discutere di pupazzi)… insomma, un sacco di gente. Con alcuni, forse troppi, le strade si sono divise, ma i ricordi rimangono indelebili.
Menzione speciale per Attila, senza il quale probabilmente non sarei qui oggi: tu sai perché.
E infine i miei genitori, Lino e Lucia, che mi hanno supportato in questo lungo percorso. Rimpiango che non ci siano le condizioni per cui possano entrambi gioire con me di questo traguardo.

Index

Introduction

As environmental concerns and energy demands increase, there is the need to move to more sustainable and flexible alternatives. One of the promising technologies in the prospect of energy sustainability is that of fuel cells, devices that convert chemical energy of a fuel into electrical energy through electrochemical processes. Despite being a technology first developed decades ago, it has been the subject of intensive research in the last years, because its full potential is far yet from being reached. Solid oxide fuel cells (hereafter called SOFCs) in particular are very promising, because their high temperature of operation leads to very high efficiencies, especially when coupled with systems that can further utilize the high quality heat that they produce.

The main goal of this work has been the development of a computational model for SOFCs at the cell level, and the study of the effect of certain significant parameters on the efficiency and power density, in order to apply it to the design and optimization of such devices. This research is parallel to one conducted by the Chemistry Department of the University of Padua, focused primarily on the development of new materials, while the engineering operating and constructive aspects of the cell can be optimized once a working computational model is used.

This thesis is divided into 4 chapters. Chapter 1 will describe the devices used, the phenomena involved and the ways in which performance can be evaluated. Chapter 2 will describe the computational model, including the geometry and the equations that constitute the system. Chapter 3 will first validate the model using a widely accepted benchmark, and then evaluate the effect that various parameters have on the overall performance of the system. Chapter 4 will simulate an Electronic Impedance Spectroscopy analysis to identify the effect that certain parameters have on the physical phenomena happening inside the cell.

Chapter 1

Solid Oxide Fuel Cells

1.1 Fuel Cells

Fuel cells are energy conversion devices that produce electrical energy directly from the chemical energy stored in the fuel through electrochemical reaction processes. They are flexible in terms of operating conditions and type of fuel used (although most operate with hydrogen, leading to the production of water). Conventional engines typically generate electrical energy from fuels in a series of energy conversion steps, which usually includes:

1. The burning of the fuel, converting its chemical energy into heat

2. The heat is then used to generated steam (steam turbines) or to increase the energy of the combusted gases (gas turbines)

3. The steam or the products of combustion are then used turbines, converting the stored heat into mechanical energy

4. Lastly, mechanical energy is used to power a generator which generates electrical power.

A fuel cell side - steps these processes, rather it generates electrical power in one single step [1, 2] without any moving parts and fewer sources of energy loss, besides not being constrained by the thermodynamics of the Carnot cycle. This leads to efficiencies of over 70% (for some type of cells), well above the limit for conventional engines. Furthermore, avoiding combustion prevents the formation of practically any pollutant, like NO_x and SO_x. They are also highly modular, and assembling small units can result in big power plants, in the order of hundreds of megawatts. Their characteristics of high energy efficiency, near zero emissions, noiseless operation, flexible sizing, fuel flexibility (for some cell types) and mechanical simplicity make them an attractive option for electrical energy generation. A typical unit fuel cell is made of three main components as shown in Figure 1.1a: anode (fuel electrode), cathode (air electrode) and electrolyte. The reactant gases are continuously supplied to the fuel and air electrodes; ions produced as a result of the electrochemical reactions migrate from one of the electrodes through the electrolyte to the other electrode. As a result of the reactions taking place, electrons are generated, these electrons flow

through an external circuit producing electric current. Unit cells are usually arranged together in series in a process called “stacking”, in other to achieve higher power capacities as depicted in Figure 1.1b

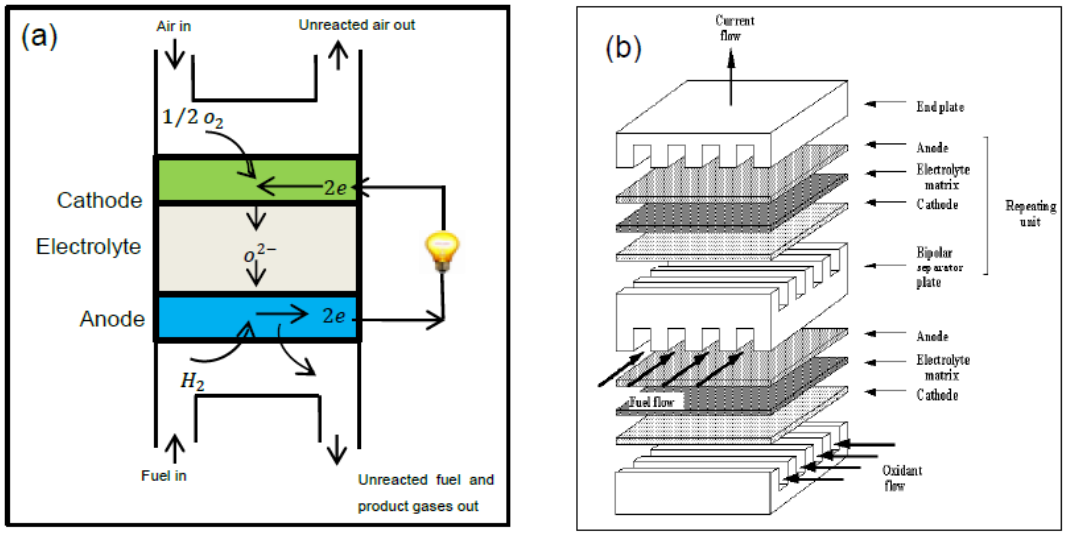

Figure 1.1. *Schematic showing the operations of a fuel cell (a) Unit fuel cell (b) Fuel cell stack*

Several types of fuel cells exist, which are classified based on the nature of the electrolyte material, which also determines the operating temperature and thus the state of reactants and products: alkaline fuel cells (50–200°C), proton exchange membrane fuel cells (30–100°C), direct methanol fuel cells (20–90°C), phosphoric acid fuel cells (200°C), molten carbonate fuel cells (200°C) and solid oxide fuel cells (600–1000°C) [1]

1.2 Solid oxide fuel cells (SOFCs)

SOFCs have a solid ceramic electrolyte, which transports oxygen ions from the cathode to the anode. The migration in the solid medium is slow, and to have acceptably low resistance, the system has to operate at high temperatures. This means that the reactants and products (water, if hydrogen is used as fuel) are in gaseous form.

SOFCs have recently gained prominence among the other fuel cell types because of the following features [4, 5]:

- Choice of fuel: SOFCs can use a wide range of fuels such as hydrogen, methanol, diesel fuel or carbon based fuels (e.g. natural gas), even accommodating the possibility of internal reforming directly within the anode [3,7]
- Efficiency: SOFCs have potentials for high electrical energy efficiencies, which increases significantly when integrated into a hybrid system that uses the high-quality waste heat produced [7]

- Constant power production: SOFCS are continuous systems, and can operate for long periods of time
- High reactive activity: electrochemical reactions in SOFCs proceed quickly due to its high operating temperature; this improves the electrode kinetics reactions (due to the large exchange currents) and reduces activation losses
- Flexibility: SOFCs are suited for a range of applications such as stationary power production, decentralized generating units, vehicular transportation (although not in small vehicles due to the high temperature required) and military applications
- Cell management: since SOFCs are solid ceramic cells, a number of the issues such as catalyst wetting, electrode flooding, electrolyte migration encountered with other fuel cells are not present.

As discussed above, SOFCs derive most of their advantages from their high operating temperature. However, this also leads to challenges associated with the development and commercialization of SOFCs. These include slow start up times, increased material and manufacturing cost due to the choice of expensive alloys such as doped lanthanum chromite ($LaCrO_3$), ceramics and gas seals that are used in the cell, issues of durability associated with thermo-mechanical stability and chemical stability due to high temperature operation, oxidizing and reducing atmospheres in the cell.
However, despite important achievements and although some SOFC systems are already commercially available, to date the breakthrough of SOFC technology still faces significant challenges concerning cost reduction, long-term stability and performance improvement. SOFCs are complex systems, involving phenomena occurring at different length scales [8]. One of the major obstacles to further significant progress is the current poor understanding of the fundamental physical and electrochemical processes and how they influence each other. For this reason, numerical models that represent the behavior of the system can be a valuable aid in identifying the effect of the phenomena involved.

1.2.1 SOFC components

A SOFC is a device made of a ceramic material electrolyte placed between two porous electrodes (anode and cathode), with interconnects on either sides that electrically connect both electrodes. For the SOFC to operate successfully, the selection of materials for the individual components is very important, both in terms of the intrinsic properties of the materials and of compatibility between them: the thermal expansion of the components should be within a small range of each other to prevent mechanical failure or delamination. Other characteristics which the material components of SOFCs should have include good chemical stability, high electrical conductivity (electrodes and interconnects), high ionic conductivity (electrolyte) and an overall low cost of production. The material choice is usually a compromise between the above characteristics. Detailed characteristics of each of the major cell components are discussed next.

Electrolyte

The electrolyte is an impervious solid made of ceramic; it is sandwiched between the anode and cathode, and its purpose is to transport oxygen ions from the anode to the cathode, while providing a physical barrier to the flow of reactants between the channels. The desired properties of electrolytes used in SOFC are mainly dictated by its high operating temperatures. A good SOFC electrolyte should have high ionic conductivity, necessary for the migration of oxygen ions through it, but it also needs to have low electric conductivity, as this forces the electrons to flow through the external circuit. Its thermal expansion should be a good match with that of other cell components, and it should be chemically stable when in contact with oxidizing and reducing environments.

Although electrolytes can be used as structural support, in which case a thickness of ~150μm is used, most research is focused on anode supported cells. In such cell configuration, the electrolyte layer is expected to be very thin, typically between 10−20 μm. At these thicknesses, there will be a significant reduction in losses due to ohmic resistance, thereby improving the cell performance.

Yttria stabilized zirconia (YSZ) is well known and used as a SOFC electrolyte. It exhibits most of the characteristics of a good SOFC electrolyte at temperatures above 700ºC.

Anode

The anode is a porous structure which experiences highly oxidizing environments. A good anode material should have high electric conductivities, necessary for the effective transportation of electrons to the interconnect. It should also have good catalyzing properties needed for the oxidation reactions taking place on it. Stability in oxidizing environments and sufficient porosity for the effective transportation of reactant gases and products are also key characteristics a good anode should have. Its thermal expansion coefficient should match those of the other components and it should have minimum or no reactivity with the electrolytes and interconnect, both of which it is in contact with it.

Most anodes are porous cermet, meaning composite materials made of sintered metallic and ceramic particles (generally nickel and YSZ [9]). This creates a continuous solid phase that transports electrons, another continuous phase that transports oxygen ions, and porous channels where gases can diffuse. The reaction occurs in the proximity of the contact perimeter between the three phases (electron-conducting, ion-conducting and gas), where the reaction participants can coexist. This is called a three-phase boundary (TPB) (Figure 1.2). In Ni/YSZ anodes, particles of YSZ are sintered with NiO, and after sintering the NiO is reduced to Ni. This means that in particular conditions, composite anodes are prone to re-oxidation, which reduces porosity and greatly affects electronic conductivity.

Cathode

The cathode is a porous material which experiences reducing environment. A good cathode material should have high electric conductivity, should be stable in reducing environments and be sufficiently porous to allow the transport of oxygen to the reaction sites. Its thermal expansion also has to be a good match with other cell components and, like the anode, it should exhibit little or no reactivity with either

the electrolyte or the interconnect. Typical material for the cathode is strontium stabilized lanthanum manganite (LSM), which is known to be a good catalyst for the dissociation of the oxygen molecule,

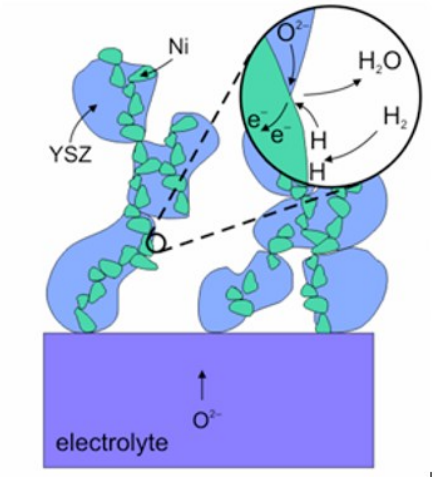

Figure 1.2. *Three-phase boundary in a composite Ni-YSZ anode*

sintered with YSZ for ionic conductivity (this produces a TPB like the one in the anode) [10]. On the opposite end of the cathode compared to the electrolyte there is a thin section of pure LSM with high porosity that acts as a current collector, gathering electrons evenly from the surface of the electrode.

Interconnect

The interconnect (also known as bipolar plate) serves as a physical barrier separating the fuel of one individual cell from the air of the neighboring one, it also conducts electric current between each layer of the cell stack and helps in distributing the reactant gases evenly across the face of the electrodes. Therefore, a good interconnect should have high electric conductivity and low contact resistance with electrodes. It should be stable in both oxidizing and reducing environments and its thermal expansion should match those of other cell components. Furthermore, the interconnect should be impermeable to the reactant gases and generally exhibit good mechanical strengths.

Metals can be used as interconnects at intermediate temperature operations; these are relatively inexpensive compared to ceramic interconnects required at high temperature operation, and are better electric conductors. Stainless steel is an attractive option because its thermal expansion matches that of YSZ [11]. However, corrosion can be a major challenge, chromium based alloys can then be used to counter this problem.

One of the layers is always much thicker than the other two, and provides structural support. The cathode is almost never used as the supporting layer, since in hydrogen-fed SOFCs it represents the main source of energy loss, given that the oxygen reduction reaction tends to be the limiting step [12-14]. As hinted above, electrolyte-supported cells are also quite rare, despite being the easiest to manufacture, because

of ohmic losses that would ensue from the conduction of ions through a thick layer. Most SOFCs tend to be anode-supported: in this case, the anode is divided into two sections, one that is highly porous and acts as the supporting layer, and a much thinner one that is where the active part where the reactions actually occur. The use of the same material as a supporting layer, despite with different porosity and average grain diameter, is justified by the need to have the same thermal expansion coefficient, lest heating results in delamination or outright fractures in the cell.

1.3 Electrochemistry

The reactions occur at the TPB where the gas meets electrode and electrolyte material. The reaction occurring at the cathode TPB is

$$\frac{1}{2}O_2 + 2e^- \rightarrow O^{2-} \tag{1.1}$$

while the following reaction occurs at the anode TPB (assuming hydrogen as fuel)

$$H_2 + O^{2-} \rightarrow H_2O + 2e^- \tag{1.2}$$

The oxygen ions are conducted through the electrolyte, while the electrons are conducted through an external electric circuit.
The overall reaction is

$$H_2 + \frac{1}{2}O_2 \rightarrow H_2O \tag{1.3}$$

The reversible voltage potential that may be supplied by the electrodes is given through the Nernst equation:

$$E^{rev} = E^0 + \frac{RT}{2F} ln\left(\frac{p_{H_2} \cdot p_{O_2}^{1/2}}{p_{H_2O}}\right) \tag{1.4}$$

with the partial pressures p in bar. E^0 is the potential at standard pressure and is determined by

$$E^0 = -\frac{\Delta G_0^f}{2F} \tag{1.5}$$

where ΔG_0^f is the change in molar Gibbs free energy of formation at standard pressure and at the actual operation temperature for the overall reaction (Eq. 1.3).

1.4 SOFC performance evaluation

There are two ways that are generally used to characterize the behavior of fuel cells and evaluate their performance. The first one is through the polarization curve, a steady-state analysis that gives the relation between voltage and current. The second one is the electrochemical impedance spectroscopy (EIS), where the inputs have an oscillating perturbation around a base value with different frequencies, and this

is helpful in the analysis of the contributions given by the various phenomena happening inside the system.

1.4.1 Polarization curve

The reversible potential E^{rev} is the maximum voltage that the fuel cell may theoretically deliver at given flow conditions. Equation 1.4 also indicates that not all the hydrogen can be utilized electrochemically, as E^{rev} approaches negative infinity for zero partial pressure of hydrogen.
If a current is flowing, the voltage supplied at the electrodes will be different from the reversible potential due to losses (also called overpotentials). The reversible potential is therefore also called "open circuit voltage" (OCV). The dependency of these losses on temperature, current density and species concentrations mainly determine the characteristics of a fuel cell. Three main mechanisms of voltage losses exist:

- Activation or polarization losses: at open circuit, no outer current is flowing. However, reactions are still taking place, but at equal rates in both directions. Just regarding the current which flows into one of the directions, we find the "exchange current density". In order to achieve an outer current higher than this, an extra potential is required to achieve the desired reaction rate, called activation voltage. The voltage drop is increasing fast at low reaction rates and is from a certain level almost constant. Activation is the dominant source of loss for low temperature fuel cells, while its influence is smaller for SOFCs.
- Ohmic losses: ohmic losses occur due to the resistance along the flow paths of electric and ionic current. At a given temperature and geometry, the voltage loss is proportional to the current.
- Diffusion or concentration losses: reactants must flow through the porous electrodes to the TPB, and products must flow into the other direction, driven by diffusion. This implies that the concentration of reactants at the TPB is lower and the concentration of products is higher than in the bulk phase. Using TPB instead of the bulk concentrations in Equation 1.4, the calculated potential will be lower and the difference is called diffusion or concentration losses. The voltage drop increases with increasing current against an asymptotic maximum current. At this point, the concentration of one of the reactants at the TPB is zero and no further current increase is possible.

Plotting the potential *vs* current behaviors of a SOFC results in what is called a polarization curve, where the effect of the different types of losses can be easily recognized (Figure 1.3).
It is immediately evident that the system presents non-linear behavior at high and low values of current density, and acts like a resistor in between extremes. It must also be noted that these curves can be generated in two different ways, varying either the voltage (galvanostatic mode) or the current density (potentiostatic mode) and recording the value of the other variable. While in steady-state operations these

two processes give the same result, this is not true for transient regimes, because of different characteristic times of the various phenomena involved.

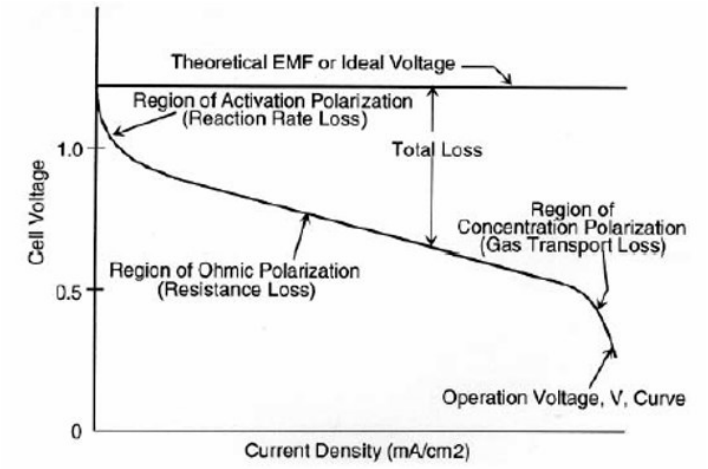

Figure 1.3. *Typical polarization curve, with sources of potential loss.*

1.4.2 Electrochemical impedance spectroscopy

Impedance measures the opposition that a circuit presents to a current when a voltage is applied. It is the extension of the concept of resistance for alternative current circuits, and unlike resistance, which only possessed a magnitude, it has both a magnitude and a phase, and is represented by a complex number.
EIS consists in using an input (either current or voltage, although galvanostatic mode is preferred in fuel cells [15]) that has small oscillating perturbations around a fixed value, with the frequency of these oscillations varying over time. Fuel cells have a behavior that is inherently non-linear; however, if the oscillations in the input are small, they act like pseudo-linear systems. By scanning the input with a wide range of frequencies, the response of the system can be recorded. This response for a given frequency will be the value of the output variable (voltage, in galvanostatic mode), shifted by a certain phase. As the input frequency varies, so does the phase shift. This is very helpful in identifying the effect of the phenomena involved: since those with long characteristic times will not perceive the effect of high-frequency oscillations, they will not influence the impedance for that frequency.
Impedance is defined as [16]:

$$Z = \frac{V_0 \sin(\omega t)}{i_0 \sin(\omega t+\varphi)} = Z_0 \frac{\sin(\omega t)}{\sin(\omega t+\varphi)} \tag{1.6}$$

By applying this signal over a spectrum of frequency, the magnitudes of various resistances and capacitances can be determined. It is expected that operating conditions, geometries, materials of construction, feed types and a variety of other fuel cell parameters will affect these impedances, just as they often affect cell power production.

Every value of the frequency gives a single point of impedance. To obtain an impedance spectrum, the frequency has to be varied over time (typically ranging from 0.1÷1 Hz to 1÷10 kHz). The plot of the imaginary vs. the real part of the impedance for all frequency values considered is called the Nyquist plot (Figure 1.4), and is characteristic of the system behavior, allowing the electrochemical phenomena analysis and their de-coupling [17].

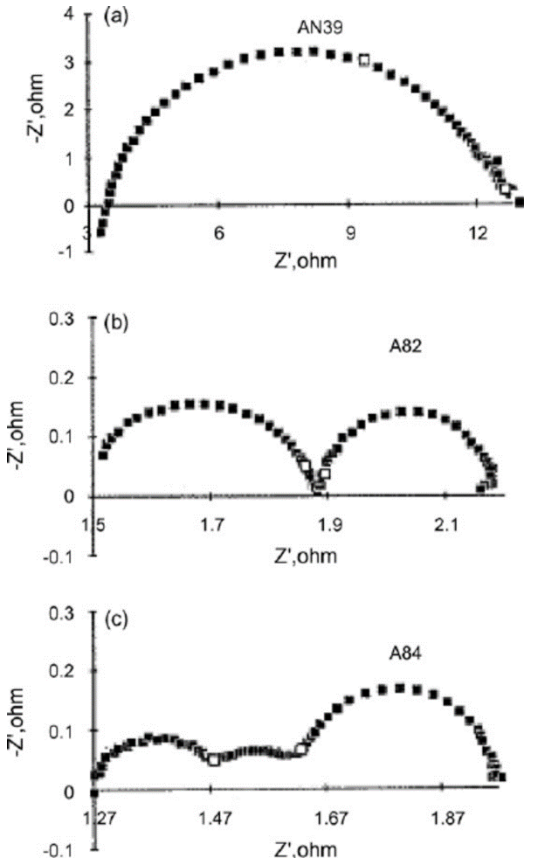

Figure 1.4 *Different types of Nyquist plots. Each point represents a specific frequency.*

In the Nyquist plot different arcs appear as a function of the phenomena occurring inside the cell (more precisely, their characteristic times: phenomena that operate on a similar timescale will be part of the same arc). This aspect will be analyzed in detail in Chapter 4.

Chapter 2

Model details and equations

SOFCs are devices where a variety of physical phenomena take place simultaneously: species and momentum transport, electro-chemical reactions, charge transport (both electric and ionic charge). In order to adequately represent such devices, a system of PDE (partial differential equations) and AE (algebraic equations) needs to be solved. This chapter describes the geometry of the system, its discretization and the equations involved.

The program used to solve the system of equations has been COMSOL Multiphysics, a finite element simulation software. [18]

2.1 Geometry

In order to validate the accuracy of the model, the geometry of the cell is that of the Forschungszentrum Jülich F–design cell, which is among the most efficient, reliable and well–characterized cells currently produced [19]. This is an anode–supported planar cell, with LSM–YSZ cathode and Ni–YSZ anode, schematically represented in Figure 2.1.

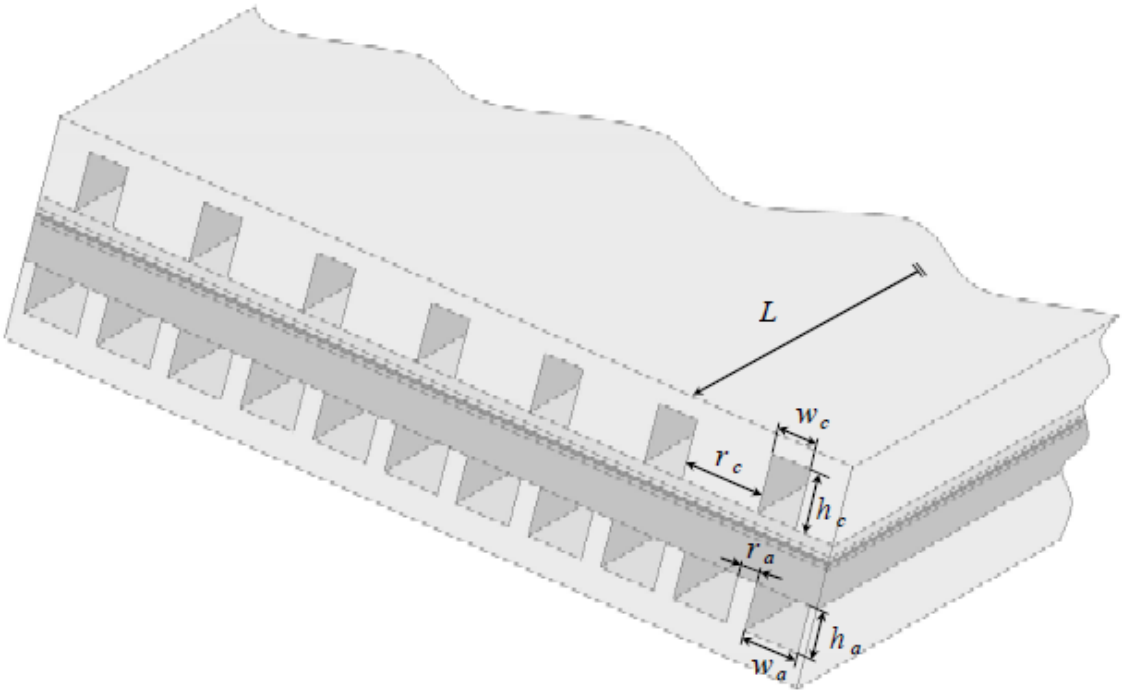

Figure 2.1. *Representation of the cell modeled in the study. The cathodic side is at the top and the anodic side at the bottom. The thickness of the active layers is not to scale.*

The whole three–dimensional structure of the stack is not represented in the electrochemical model: for computational reasons, only a 2D slice of a cell along the length *L*, representative of the repeating unit of the SOFC system, is considered (Figure 2.2). While this approach does not consider some details, such as the uneven distribution of gases and current under the ribs [20, 21], it is still able to capture the main characteristic phenomena occurring in the system, while at the same time keeping the computational costs reasonable.

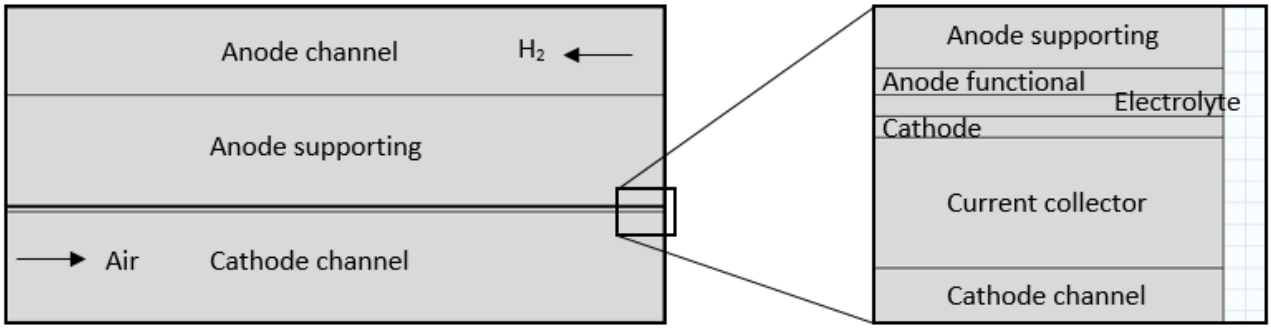

Figure 2.2. *Geometry used in the simulation, with detail of the active layers (proportions are off for visualization purposes: the entire cell is 4.292 mm high and 90 mm long).*

In Figure 2.2, the bottom domain is the cathode channel, where air is fed, while the top domain is the anode channel, fed with hydrogen. The anodic supporting layer is formally part of the anode, being made of the same material (albeit with different porosity), and its purpose is to confer the cell structural integrity while not being an active part of the reactions itself. These three domains are by far the thickest, which is why a magnification is necessary to identify the other layers, which are the most important ones for the process. Above the cathode channel the current collector, then the cathode, the electrolyte and the functional part of the anode. The details and function of the different layers will be described in the following paragraph.
The 3-D stack of cells considered is a square with nominal dimension 100mm x 100mm, where the active part is actually 90mm x 90mm, therefore the longitudinal dimension of the model is 90mm.

2.1.1 Domains

The channels for gas flow are empty, and the only relevant parameter is their height: the cathode channel is 1.5mm high, whereas the anode channel is slightly smaller, 1.2mm.
As for the layers of the cell itself, we have, starting from the bottom, the cathode current collector, which is a porous layer of LSM whose purpose is to evenly distribute electric current along the surface of the electrode. It also adds some structural resistance to the cathodic side of the cell.

Then there is the cathode, a LSM/YSZ composite material, where the oxygen reduction reaction happens. The next layer is the electrolyte, which is a dense phase of pure YSZ that blocks the flow of gases and is electrically insulating, thus forcing the current to flow through an external circuit, while being able to conduct oxygen ions from the cathodic side of the cell to the anodic one.
Above the electrolyte there is the functional layer of the anode, with a smaller porosity in order to maximize the length of TPB per unit volume, where the fuel is oxidized.
Finally, there is a thick anodic layer that acts as structural support, while not taking part in the actual reactions. This layer needs to be porous enough to offer a small resistance to the diffusion of gases, while maintaining structural integrity. It is made of the same material as the actual anode only to minimize the chances of mechanical failure or delamination due to thermal expansion.
The morphological and geometrical input parameters are reported in Table 2.1.

Table 2.1. *Details of the layers of the cell simulated in this study.*

Parameter	***Current collector***	***Cathode functional layer***	***Electrolyte***	***Anode functional layer***	***Anode supporting layer***
Material	LSM	LSM/YSZ	YSZ	Ni/YSZ	Ni/YSZ
Ψ_{el}	1 [22]	0.475* [22]	0.0 [22]	0.397# [23]	0.397# [23]
ϕ	0.42 [24]	0.42 [22]	0.0 [22]	0.235 [23]	0.43 [23]
Thickness [μm]	60	10	10	12	1500

* Corresponding to LSM - YSZ 50 - 50% in weight.
# The anodic layers are obtained by sintering NiO and YSZ particles, and then reducing NiO to Ni. The corresponding fraction of NiO - YSZ before reduction is 56 - 44% in weight.

2.2 COMSOL modules

The following modules have been used in the simulation. The equation that are solved by the software are detailed in the next paragraph.

Free and Porous Media Flow. This is applied to the cathode side (cathode channel, current collector and cathode) and the anode side (anode channel, anode supporting and anode functional), and is used to compute fluid velocity and pressure fields of single-phase flow where free flow is connected to porous media. This module is well suited for transitions between slow flow in porous media, governed by the Brinkman equations, and fast flow in empty channels described by the Navier-Stokes equations. The required inputs are:

- Fluid density
- Fluid viscosity
- Inlet velocity

- Inlet pressure
- Porosity of the porous phase (or phases, if they have different porosity like in the anode side)
- Permeability of the porous phase(s).

Transport of Concentrated Species. Again this physics is applied to both the anode and the cathode side (meaning, everything above and below the electrolyte, including the gas channels). It is used to study gaseous mixtures where the species concentrations are of the same order of magnitude, and none of the species can be identified as a solvent. In this case, properties of the mixture depend on the composition, and the molecular and ionic interactions between all species need to be considered. The physics interface includes models for multicomponent diffusion, where the diffusive driving force of each species depends on the mixture composition, temperature, and pressure. Among the different option available to model the diffusion of the species, the Stefan-Maxwell model has been selected, since it is more accurate despite the increased computational cost. Results with other diffusion models like Fick's law or mixture average differ in a slight but noticeable manner, making Stefan-Maxwell the preferred choice. An alternative approach to the diffusion mechanism would have been the dusty-gas model, which includes convection and both ordinary and Knudsen diffusion [25, 26]. This model has been found to be more accurate in the prediction of mass transport in SOFC electrodes [27], but it is not available in the COMSOL module, and attempts to implement it via an external function caused numerical instability issues and had to be abandoned. The required inputs are:

- Temperature
- Pressure
- Velocity field
- Binary diffusion coefficients for hydrogen – water vapor on the anode side, and nitrogen – oxygen on the cathode side
- Molecular weights of the species
- Density equation of state (given the high temperature, ideal gas law is a very reasonable assumption).

Secondary Current Distribution. This module defines the transport of charged ions in an electrolyte of uniform composition, as well as current conduction in electrodes using Ohm's law in combination with a charge balance. It accounts for activation overpotentials, but it is possible to correct it with a term that also considers concentration overpotentials. It is applied to the whole cell (excluding the gas channels), although the reaction kinetics are only limited to the active layers (cathode and functional part of the anode). The required inputs are:

- Electric and ionic conductivities of the different layers

- TPB length per unit volume (the module actually requires an active specific area, but it is possible to manipulate the equations in order to apply them to a length over volume)
- Kinetic expressions for the electrochemical reactions.

2.2.1 Coupling between modules

The three modules used (actually, five, since the Free and Porous Media Flow and the Transport of Concentrated Species are used twice, once for the anode side and once for the cathode) are not independent from each other. Several inputs on a module are outputs of another one. Specifically:

- The Free and Porous Media Flow modules have the density value that is determined by the results of the Transport of Concentrated Species modules, and the generation terms that depend on the local current density.
- The current density itself is a function of the concentrations of species given by the Transport of Concentrated Species modules, coupling them with the Secondary Current Distribution module.
- The Transport of Concentrated Species modules use pressure and velocity fields that are calculated through the Free and Porous Media Flow module.

Figure 2.3 reports a schematic representation of the modules used in each domain, as well as the properties that couple the considered modules.

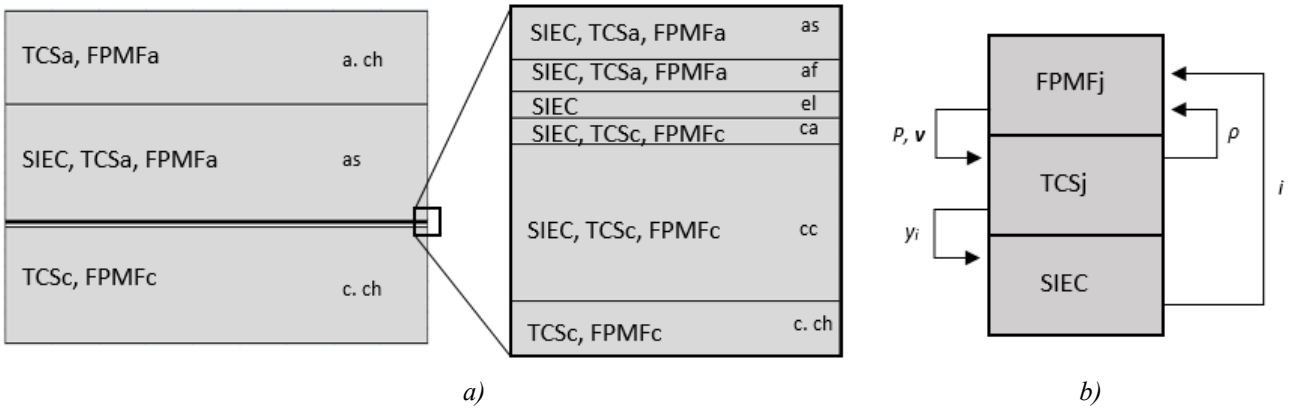

a) *b)*

Figure 2.3. *a) Representation of the modules used in each domain (a. ch = anode channel, as = anode supporting, af = anode functional, el = electrolyte, ca = cathode, cc = current collector, c. ch = cathode channel). b) Interactions between modules. PFMFj = Porous and Free Media Flow module (j = a, c), TCSj = Transport of Concentrated Species module (j = a, c), SIEC = Secondary Current Distribution module.*

2.3 Assumptions, equations, boundary conditions, properties

2.3.1 Assumptions

The model uses the following assumptions, that allow to considerably simplify the equations while maintaining accuracy in the representation of the phenomena:

- Fixed and even temperature. While the global reaction is an oxidation and therefore exothermic, the conversion is not very high, and does not influence the temperature significantly. In reality, cell stacks like these are kept at constant temperature in an oven, and the temperature inside the system can be considered uniform (high temperature gradients will likely damage the fragile ceramic materials). Investigations into temperature gradients inside the cell [28] proved experimentally that the increase in cell temperature with increasing current density (up to 1A/cm^2) was quite similar in all the test conditions and restricted to 10–20°C with respect to the operating temperature at OCV. In addition, they verified that no particular variation in temperature between different cells within a stack was evident, and therefore the effect of larger thermal gradients could be neglected. Therefore, the conservation of energy has not been taken into account.
- Ideal gas law. The cell operates at atmospheric pressure (at the inlet), and at high temperature (the base case is at a temperature of 800°C), so this assumption is quite reasonable.
- Porous phase modeled as a continuum. The porous matrixes are consider isotropic and are characterized only by their porosity and permeability. Similarly, it is assumed that the length of TPB per unit volume is constant throughout the electrode (for the anode, only the functional part of the electrode is considered)
- Steady-state or quasi steady-state. The simulations have been conducted either under constant inputs, or with small oscillations around a fixed value. Degradation of material properties over time has not been taken into account, despite the fact that currently SOFCs maintain their properties for a relatively short time (measured in months or years, not decades).

2.3.2 Equations

Free and Porous Media Flow module

Momentum conservation equations in the Free and Porous Media Flow module consider Navier-Stokes equations for empty channels (Eqs. 2.1, 2.2), and Brinkman equation for the porous region (Eqs. 2.3, 2.4), imposing continuity at the interface:

$$\rho\nabla\mathbf{u} = 0 \tag{2.1}$$

$$0 = -\nabla P + \nabla\mu(\nabla\mathbf{u} + (\nabla\mathbf{u})^T) \tag{2.2}$$

$$\rho\nabla\mathbf{u} = Q_{br} \tag{2.3}$$

$$0 = -\nabla P + \nabla\left[\frac{1}{\varepsilon}\left\{\mu(\nabla\mathbf{u} + (\nabla\mathbf{u})^T) - \frac{2}{3}\mu\nabla\mathbf{u}\right\}\right] - \left(\frac{\mu}{\kappa} + \frac{Q_{br}}{\varepsilon^2}\right)\mathbf{u} \quad (2.4)$$

Q_{br} is a term that considers the productions and consumption of matter: in the porous matrix there is a reaction that violates the conservation of matter, since oxygen ions "disappear" from one channel and "reappear" on the other one, conducted by the solid phase, and this influences the momentum conservation equations.

Transport of Concentrated Species module

The transport of species is governed by the basic equation:

$$\nabla(\rho w_i \boldsymbol{u}) = -\nabla \boldsymbol{j_i} + R_i \quad (2.5)$$

When using the Stefan – Maxwell diffusion model, the relative mass flux vector is:

$$\boldsymbol{j}_i = -\rho w_i \sum_{k=1}^{Q} D_{ik}\boldsymbol{d}_k \quad (2.6)$$

This assumes to neglect thermal diffusion, and uses diffusion coefficients that are already considering the porosity of the porous matrix. The diffusional driving force, if forces for unit mass (like the effect of gravity or charged species in an electric field) are neglected, is expressed by:

$$\boldsymbol{d}_k = \nabla x_k + \frac{1}{P}[(x_k - w_k)\nabla P] \quad (2.7)$$

The rate of production/consumption of species is:

$$R_i = MW_i \sum_m a_m \frac{\nu_{i,m} i_m}{n_m F} \quad (2.8)$$

Notice that the software requires a value for the current surface density and for the specific area for the reaction. The nature of the reaction in a SOFC implies that the reaction takes place on a length per unit volume, and is driven by a current linear density. However, multiplying one term and dividing the other for the same arbitrary length, the end result is identical and can be implemented in the model without requiring an overhaul of the equations used by it.

Secondary Current Distribution module

The transport of charged species is assumed to follow Ohm's law, both for electric and ionic conduction. At the anode, for the electrons:

$$\nabla N_e = a_a \frac{i_a}{F} \quad (2.9)$$

$$N_e = \frac{\sigma_{el,a}\chi_{el,a}^{eff,a}}{F}\nabla V_{el,a} \quad (2.10)$$

Once again the first equation can be used also with a current linear density and a length for unit volume. In an analogous manner, for the oxygen ions the governing equations are:

$$\nabla N_O = a_a \frac{i_a}{2F} \tag{2.11}$$

$$N_O = \frac{\sigma_{io}\chi_{io}^{eff,a}}{2F}\nabla V_{io} \tag{2.12}$$

In both sets of equations the effective conductivity takes into account that in a porous matrix the conductivity is significantly lower than what it would be in a dense medium. Equations 2.9 - 2.12 apply to both the supporting and the functional layer of the anode (with different values for intrinsic properties). For the cathode, the conduction of species is given by:

$$\nabla N_e = -a_c \frac{i_c}{F} \tag{2.13}$$

$$N_e = \frac{\sigma_{el,c}\chi_{el,c}^{eff,c}}{F}\nabla V_{el,c} \tag{2.14}$$

$$\nabla N_O = a_c \frac{i_c}{2F} \tag{2.15}$$

$$N_O = \frac{\sigma_{io}\chi_{io}^{eff,c}}{2F}\nabla V_{io} \tag{2.16}$$

The current collector is a purely electric conducting phase, with no TPB and no consequent production or consumption of species, therefore the only equation governing it is:

$$N_e = \frac{\sigma_{el,c}\chi_{el,c}^{eff,cc}}{F}\nabla V_{el,c} \tag{2.17}$$

For the electrolyte, only ionic conduction is considered since it is an electrical insulator (the material of which the electrolyte is made actually has a very small electric conductivity, but this is so small that the current flows almost exclusively through the external circuit, and therefore its value has been neglected in the model):

$$\nabla N_O = 0 \tag{2.18}$$

$$N_O = \frac{\sigma_{io}}{2F}\nabla V_{io} \tag{2.19}$$

The current densities values that appear in the transport equations above are determined by the reaction kinetics. At the anode, the kinetic expression is a modified version of the Butler-Volmer equation, in which the current density is a function of the anodic activation overpotential [29, 30]. There is also a term correcting the equation for the hydrogen adsorption/desorption equilibrium (which is a constant, at a given temperature):

$$i_a = i_{0a}\left\{\exp\left[(1+\alpha_a)\frac{F\eta_a}{RT}\right] - \exp\left[(1-\beta_a)\frac{F\eta_a}{RT}\right]\right\} \tag{2.20}$$

$$i_{0a} = i_{0a}^{ref} \exp\left[-\frac{E_a^{act}}{R}\left(\frac{1}{T} - \frac{1}{T_a^{ref}}\right)\right] \frac{\left(\frac{P_a y_{H_2}}{P_{H_2}^*}\right)^{\frac{1-\alpha_a}{2}} \left(\frac{P_a\left(1-y_{H_2}\right)}{P_{atm}}\right)^{\frac{1+\alpha_a}{2}}}{1+\left(\frac{P_a y_{H_2}}{P_{H_2}^*}\right)^{0.5}} \tag{2.21}$$

$$P_{H_2}^* = \frac{A_{des}\Gamma^2\sqrt{2\pi RT\mathrm{MW}_{H_2}}}{\gamma_0} \exp\left(-\frac{E_{des}}{RT}\right) \tag{2.22}$$

$$\eta_a = -\frac{RT}{2F} \ln\left(\frac{y_{H_2,in}}{y_{H_2}} \frac{1-y_{H_2}}{1-y_{H_2,in}}\right) - \left(V_{io} - V_{el,a}\right) \tag{2.23}$$

A similar approach is used at the cathode side for the description of the oxygen reduction reaction. Here a Butler–Volmer expression is used [31] where the exchange current density depends on the local oxygen partial pressure, while the activation overpotential comprises both the potential difference between conducting phases and the equilibrium potential step. The sign convention is coherent with the one used in Eq. 2.20, that is, a positive activation overpotential leads to a positive current density representative of oxygen consumption:

$$i_c = i_{0c}\left\{\exp\left[(1+\alpha_c)\frac{F\eta_c}{RT}\right] - \exp\left[(1-\beta_c)\frac{F\eta_c}{RT}\right]\right\} \tag{2.24}$$

$$i_{0c} = i_{0c}^{ref} \exp\left[-\frac{E_c^{act}}{R}\left(\frac{1}{T} - \frac{1}{T_c^{ref}}\right)\right]\left(\frac{P_c\, y_{O_2}}{P_{O_2}^{ref}}\right)^{\zeta} \tag{2.25}$$

$$\eta_c = -\frac{RT}{4F} \ln\left(\frac{P^{in} y_{O_2,in}}{P\, y_{O_2}}\right) - \left(V_{el,c} - V_{io}\right) \tag{2.26}$$

It is worth noticing that while Eqs. 2.1 – 2.19 are valid for any SOFC with porous composite electrodes and no mixed (i.e. ionic and electric) conduction, Eqs. 2.20 – 2.26 are strictly valid for the couples of materials considered, i.e. Ni/YSZ and LSM/YSZ, since they represent global kinetic expressions derived and validated exclusively for those materials.

2.3.3 Boundary conditions

At the inlet of the channels, boundary conditions are pressure, velocity and hydrogen or oxygen molar fraction. Open boundary conditions at the outlets are used. For the cell, at the electrolyte-electrode (anode or cathode) interface no-flux conditions are applied to gas species and electrons, given that the electrolyte is a dense, electrically insulating material. Similarly, no-flux for oxygen ions is applied to the supporting

anode – anode channel interface, and the cathode – current collector interface (the current collector is made of a purely electrical conductor).

The absolute electric potential is determined up to an additive constant, and therefore the potential at the current collector – cathode channel interface is set arbitrarily at 0. At the anode side (supporting anode – anode channel interface), the cell potential V_{cell} is imposed as a boundary condition. Specifically, the

electric potential of the electron – conducting phase is set as $V_{ela} = \eta_{cell}$, where η_{cell} represents the cell overpotential, defined as:

$$\eta_{cell} = OCV - V_{cell} \tag{2.27}$$

The OCV is given by the Nernst equation [1]:

$$OCV = E^0 - \frac{RT}{2F} \ln \left[\frac{1-y_{H_2,IN}}{y_{H_2,IN}} \left(\frac{P_{c,IN}}{P_{c,IN} \cdot y_{O_2,IN}} \right)^{1/2} \right] \tag{2.28}$$

It is worth noting that $V_{ela} = \eta_{cell} = 0$ at open circuit conditions. Similarly, the electric potential of the ion – conducting phase V_{io} is the relative potential that equals 0 at open circuit conditions. Using reference potential corresponds to shifting them by a constant reference [32], which does not influence the output of the model.

The model validation is performed against experimental polarization curves [35] obtained with the operating conditions reported in Table 2.2, which are therefore those used for the base case in this study.

Table 2.2. *Operating conditions used for model validation against literature data.*

Parameter	*Value*
T	800°C
$P_{a,IN}$	1 atm
$P_{c,IN}$	1 atm
$y_{H2,IN}$	0.965
$y_{O2,IN}$	0.210
v_{fuel} *	1.617 m/s
v_{air} *	3.639 m/s

** these correspond to flow rates of 8 NL/min and 10 NL/min for fuel and air respectively.*

Table 2.3 contains the permeability, the effective conductivity factors and the length of TPB per unit volume in the different layers. Note that the electrolyte parameters are not there since the effective conductivity is 1 and the permeability is 0 (it is a dense phase), and there is no TPB.

Table 2.3. *Microstructural properties for the cell layers (n/a means not available, but irrelevant for the study since there is no reaction or ion conduction in the supporting anode layer)*

Parameter	*Current collector*	*Cathode*	*Anode Functional*	*Anode supporting*
κ	$1.874 \cdot 10^{-1}$ [36]	$2.557 \cdot 10^{-4}$ [36]	$1.667 \cdot 10^{-4}$ [36]	$1.2 \cdot 10^{-2}$ [37]
χ_{el}^{eff}	0.1944 [36]	0.0095[36]	0.0282 [36]	0.0346 [37]
χ_{io}^{eff}	/	0.0382 [36]	0.1239 [36]	n/a
λ_{TPB}	/	4.608	3.243	n/a

These boundary conditions mathematically close the model. In addition, several expressions have been used to calculate physical and electrochemical properties. Those expressions, and a series of parameters specific to the materials considered, are reported in Table 2.4.

Table 2.4. *Physical and electrochemical properties for the gas species (H2, O2, H2O, N2) and conducting materials (LSM, YSZ, Ni) used in this study.*

Parameter	*Value or Expression*	*Reference*
Gas phase properties		
μ_a	$\frac{y_{H_2}\mu_{H_2}M_{H_2}^{0.5} + (1-y_{H_2})\mu_{H_2O}M_{H_2O}^{0.5}}{y_{H_2}M_{H_2}^{0.5} + (1-y_{H_2})M_{H_2O}^{0.5}} \frac{kg}{m\cdot s}$	[32]
μ_c	$\frac{y_{O_2}\mu_{O_2}M_{H_2}^{0.5} + (1-y_{O_2})\mu_{N_2}M_{N_2}^{0.5}}{y_{O_2}M_{O_2}^{0.5} + (1-y_{O_2})M_{N_2}^{0.5}} \frac{kg}{m\cdot s}$	[32]
D_{H_2,H_2O}	$\frac{0.0143\cdot T^{1.75}}{P_a(6.12^{1/3}+13.1^{1/3})^2}\sqrt{\frac{1/M_{H_2}+1/M_{H_2O}}{2000}} \frac{m^2}{s}$	[32]
D_{O_2,N_2}	$\frac{0.0143\cdot T^{1.75}}{P_c(16.3^{1/3}+18.5^{1/3})^2}\sqrt{\frac{1/M_{O_2}+1/M_{N_2}}{2000}} \frac{m^2}{s}$	[32]
Solid phase properties		
σ_{ela} (Ni)	$3.27\cdot 10^6 - 1065.3\cdot T \ \frac{S}{m}$	[33]
σ_{elc} (LSM)	$8.855\cdot 10^7 \frac{\exp\left(-\frac{1082.5}{T}\right)}{T} \frac{S}{m}$	[33]
σ_{io} (YSZ)	$3.34\cdot 10^4 \exp\left(-\frac{10300}{T}\right) \frac{S}{m}$	[33]
E^0 (800°C)	0.978 V	[1]
Anode kinetics		
i_{0a}^{ref}	$4.092\cdot 10^{-2} \ \frac{A}{m}$	[29]
α_a	0.3	[29]
β_a	0.7	[29]
E_a^{act}	$120 \ \frac{kJ}{mol}$	[31]
T_a^{ref}	700°C	[29]
A_{des}	$5.59\cdot 10^{15} \ \frac{m^2 s}{mol}$	[34]
E_{des}	$88.12 \ \frac{kJ}{mol}$	[34]
Γ	$2.6\cdot 10^{-5} \ \frac{mol}{m^2}$	[34]
γ_0	0.01	[34]
Cathode kinetics		
i_{0c}^{ref}	$2.5\cdot 10^{-4} \ \frac{A}{m}$	[20]
α_c	1.5	[20]
β_c	0.5	[20]
E_c^{act}	$140 \ \frac{kJ}{mol}$	[20]
T_c^{ref}	945°C	[20]
$P_{O_2}^{ref}$	0.21 atm	[20]
ζ	0.375	[20]

For the simulations under perturbations, the potential imposed as a boundary condition oscillates with time, according to the law:

$$V_{cell,t} = \eta_{cell} + \Delta V \exp(-i\omega t) \quad (2.29)$$

As discussed, ΔV is small enough (10 mV) that the system response to the perturbation is pseudo – linear.

2.4 Meshing

COMSOL is a finite element solver, which means that the domain is discretized into small sub – domains in which PDEs are locally approximated to AEs for steady – state problems and ODEs for transient problems.

In this study, the longitudinal gradients are less important that the transversal ones, so a mapped rectangular mesh with a prevalent dimension along the length of the cell has been selected. To more carefully represent the transitions at the interfaces, which proved to be critical for the numerical stability of the model, the height of the mesh decreases the closer the sub – domains are to the interfaces (Figure 2.4). This allowed for a detailed description of the system without adding too much computational cost (a total of 46,000 domains has been mapped).

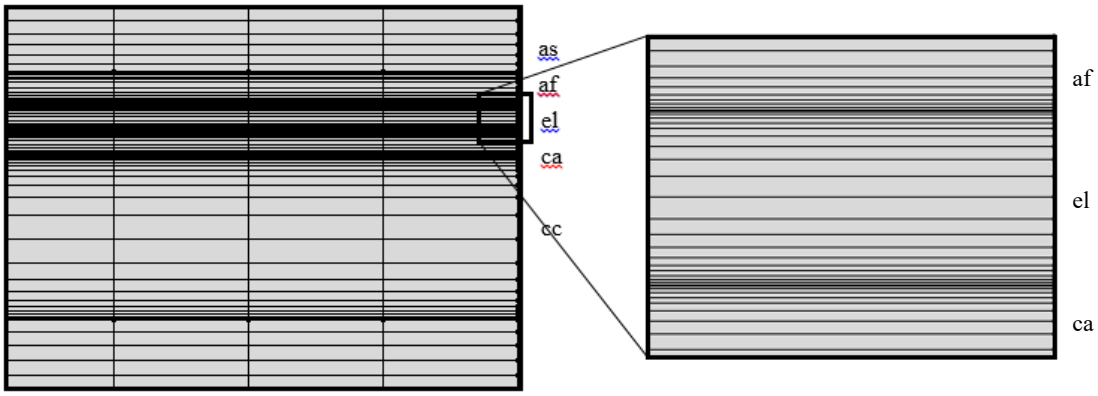

Figure 2.4. *Meshing of the central layers of the cell (as = anode supporting, af = anode functional, el = electrolyte, ca = cathode, cc = current collector), with a detail of the anode – electrolyte – cathode interfaces to highlight the increased detail of description close to the interfaces.*

Sensitivity analyses on the number of domains showed that adding more detail does not improve the results, meaning that the selected meshing is adequate to describe the system accurately. In particular, quadrupling the domains to 184,000 (halving the domain sizes in both directions) yielded results which were indistinguishable from those detailed in the following Chapters.

Chapter 3

Model validation and parametric analysis

In this chapter the model used in this study is first validated against experimental data, and then used to predict the effect that modifying certain parameters has on the cell performance.
First, however, it is useful to discuss in more detail the polarization curves, which will be the tools used to evaluate performance in this chapter.

3.1 Polarization curve

At open circuit conditions, a fuel cell (or, in general, any electrochemical device) displays an electromotive force that corresponds to the variation of free energy of the global reaction, divided by the number of exchange electrons and Faraday's constant. When the circuit is closed and current starts to flow through the system, this is no longer in equilibrium and a phenomenon called polarization ensues, which reduces the available electromotive force. The difference between the actual cell potential and the theoretical, reversible potential is called overpotential. It is worth noticing that the cell overpotential is the sum of the overpotentials at the two electrodes, although the contribution of each electrode to the total overpotential is not immediately discernible.
Conduction of electrons and oxygen ions, that start to flow once the circuit is closed, is subjected to internal electrical resistances. These can be independent on the flow of current (ohmic resistance of the electrodic and electrolytic materials) or dependent on it (electronic transfer and matter transfer). Therefore, while ohmic resistance is a relevant factor regardless of the exchange current density, other phenomena are more prevalent at low or high current densities. A breakdown of the various contributions and be see in Figure 3.1.
One resistance that is always relevant, but more so at low current densities, is the activation overpotential. This is due to the resistance to the transfer of electrons in the electrochemical reactions, which means the slow speed of the reactions (since current density is the driving force of said reactions, it is to be expected that this source of potential loss is more relevant at low current densities). Activation overpotentials exist for both the anode and the cathode. However, the oxygen reduction is by far the slower process, and contributes to almost the totality of activation losses. In fuel cells operating at lower temperature (i.e. lower reaction rates), the activation losses are the dominant contribution to the total overpotential. While the high operating temperature in SOFCs leads to faster reactions and therefore smaller activation overpotentials, the contribution of electron transfer to the total potential losses is still significant.

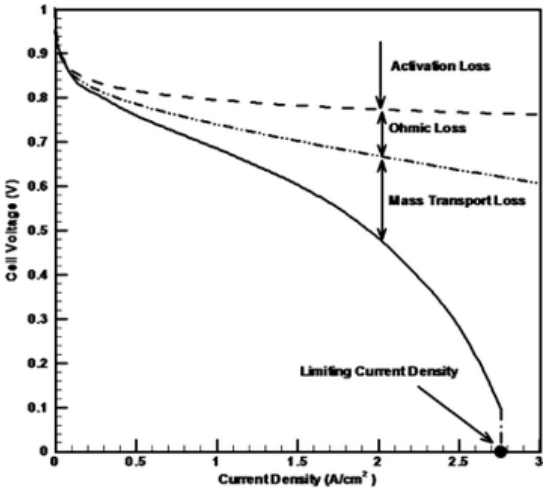

Figure 3.1. *Breakdown of potential losses into the contributions of activation overpotential, ohmic resistance and concentration overpotential.*

At high current densities, there is another source of potential losses, associated with the transport of species via diffusion that cannot match the high reaction rates, called concentration (sometimes diffusion or mass transport) overpotential. When the circuit is open, the concentration of reacting species at the TPB is constant (the system is in dynamic equilibrium, so the rates of consumption and production are the same). When current flows, this leads to a concentration gradient near the electrode, which means that the reactants have to diffuse through the porous matrix towards the TPB in order to react. Therefore, the concentration at the TPB will be much smaller than the one in the bulk. The larger the exchange current, the faster the electrochemical reaction is and the larger the concentration gradient becomes, so the contribution of concentration overpotential becomes more pronounced.

These contributions are reflected in the shape of the polarization curve like Fig 3.1, which is a plot of the cell voltage *vs.* the current density. This is fairly linear in the central part, while at low current densities the shape is heavily influenced by the activation overpotential, and at high densities by the concentration overpotential.

In order to obtain an experimental polarization curve, the cell has to be operated at different values of either current or voltage, recording the values of other variable. As noted in Chapter 1, this can be done in galvanostatic mode (varying the current) or potentiostatic mode (varying the voltage). For steady-state operations, which are the conditions in which the polarization curve is measured, these two modes give the same results. The model implemented in this study also operates under stead-state assumptions in determining polarization curves, although it is coded for potentiostatic mode.

3.2 Model validation

In order to ensure that the model developed in this study accurately represents the physical phenomena involved in a fuel cell, it has to be compared to experimental data. The geometry of the system is that of a well-know and studied commercial fuel cell, the Forschungszentrum Jülich in the F design, and the operating conditions used as boundary conditions as detailed in the previous Chapter have been chosen to match those used in experimental tests with this type of cell [35]. This allows for a direct comparison between the experimental polarization curve and the simulated one. The results of this comparison are shown in Figure 3.2.

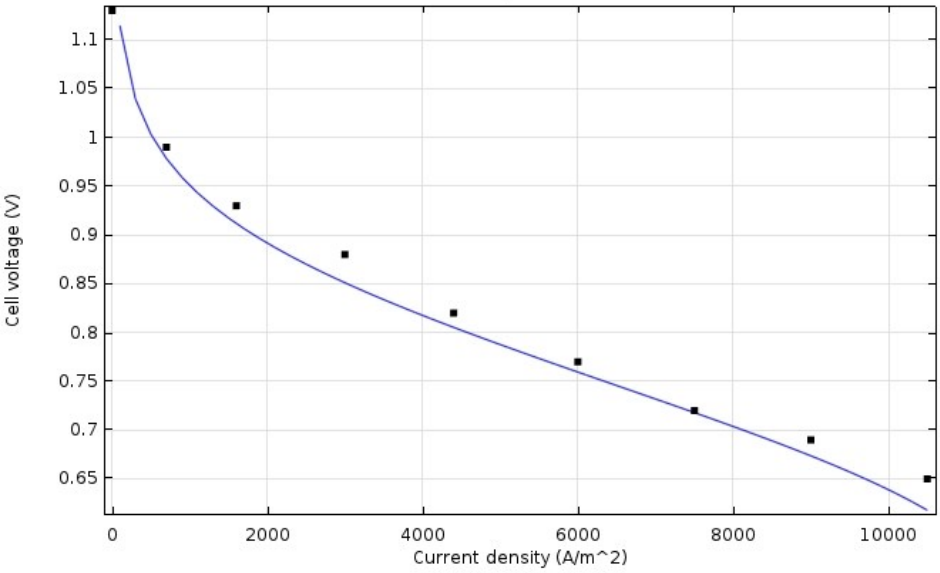

Figure 3.2. *Simulated polarization curve and comparison with experimental data.*

There is some difference with experimental data, probably due to a few of the assumptions and simplifications of the simulation as well as the use of the Stefan – Maxwell diffusion model instead than the more accurate dusty – gas model, but the representation of the physical behavior is adequate enough to affirm that the model can be used as a valuable tool in the design and optimization of fuel cells.

It is worth mentioning that this is not a fitting. There are no adjustable parameters that have been fitted to the experimental data, the simulated polarization curve is exclusively a product of the geometry, the operative conditions, the microstructural data and the kinetic parameters, all of which are an input to the simulation. The relative accuracy with which the experimental data are reproduced without the need for adjustable parameters is a good indication that the model is able to adequately reproduce the phenomena occurring inside the cell.

Another indication of the model's accuracy can be obtained by plotting the fuel molar fraction in the channel, and confronting the exit value with literature data containing a value for the fuel utilization factor [38]. This quantity is defined as the sum of the molar flow rates of every species that could act as a fuel at the inlet, multiplied by its enthalpy, and divided by the same quantity at the outlet. It os mainly

useful when different fuels are fed to the cell, or when internal reactions like reforming transform one fuel into another. For a single fuel like the one used in these simulations, this becomes the fuel conversion. For this comparison, the operating conditions for the model have been varied from those detailed in Chapter 2 to match those that were used to obtain experimental data (in particular, an excess of oxygen was used). The results of the simulation can be seen in Figure 3.3.

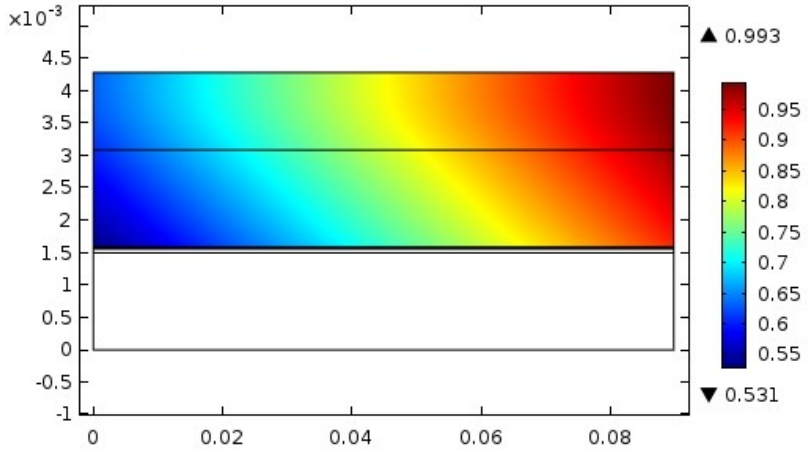

Figure 3.3. *Hydrogen molar fraction in the anode side of the cell*

This composition profile is in agreement with a data of 0.408 for the fuel utilization factor (meaning the hydrogen conversion, since there are no other species that can act as fuels in the channel). Using a boundary probe to integrate the species flow rate over the entire section of the anode channel outlet, and calculating the hydrogen conversion (the flow rate of fuel at the inlet is known, velocity and composition are inputs of the simulation), the resulting value is 0.39016, slightly different from the experimental data but within a reasonable margin of error.

3.3 Overpotential breakdown

Normally, when conducting experiments, only the total polarization curve can be obtained. Although the causes of the non-linearity of the curve are known, it is not easy to break down the various contributions. There are however theoretical models that isolate the contributions of overpotentials. A simplified one is:

- Activation overpotential [39]:

$$\eta_{act} = \frac{R\,T}{1.4\,F}\ln\left(\frac{i}{i_{act}}\right) \tag{3.1}$$

- Ohmic overpotential:

$$\eta_{ohm} = R_{ohm}\cdot i \tag{3.2}$$

- Concentration overpotential [40]:

$$\eta_{conc} = -\frac{R\,T}{2\,F}\ln\left(1-\frac{i}{i_{conc}}\right) \tag{3.3}$$

- Total cell polarization

$$V_{cell} = OCV - \eta_{act} - \eta_{ohm} - \eta_{conc} \tag{3.4}$$

This model includes 3 adjustable parameters. However, these can be obtained by the fitting of the simulated curve, whose validity has already been verified against experimental data. This allows to break down the various contributions. Furthermore, the model can extend the polarization curve beyond the inputs used in the literature data used to validate it. Results of this are reported in Figure 3.4.

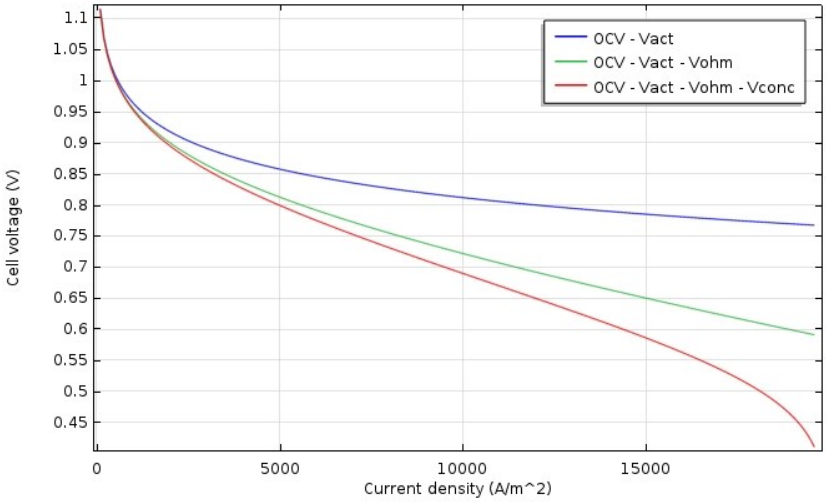

Figure 3.4. *Contributions to the total overpotential.*

Figure 3.4 is qualitatively equivalent to Figure 3.1, which was used to illustrate the concept of overpotentials. However, this breakdown is quantitative in nature, resulting from the actual model of the cell. The activation overpotential obviously plays a big role in the total losses, especially at low current densities. At higher current densities, the contribution of the concentration overpotential becomes more relevant, and the deviation from linearity can be seen more clearly than in Figure 3.2.

Since fuel cells' purpose is to generate electrical power, it can also be useful to plot the power density generated (voltage · current density) vs. the current density. This is done in Figure 3.5.

It is worth noticing that the power generated reaches a maximum value, and the decreases. This is due to potential losses from concentration gradient becoming more and more relevant at high current densities, so a small increase in current density is associated with a rather large drop of cell voltage, resulting in less power produced. It also means that there is an optimal current density (or potential) at which to operate the cell. This was not immediately clear by looking at the data used to validate the model [35], as the available current density values were all in the region where power increases with current density. There is however a reason why the current density should not exceed a certain value, and the potential in the experimental data was not set below 0.6 V, and that is the reoxidation of the anode at high current

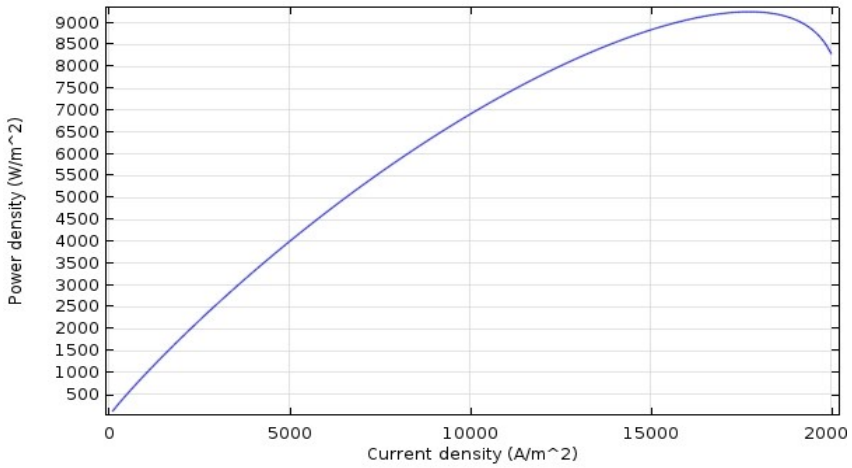

Figure 3.5. *Power density output vs. current density.*

densities [41]. At lower potentials, the oxygen ions conducted through the ion-conducting phase can react with nickel particles in the composite anode, oxidizing them to NiO instead of reacting with the hydrogen. Different materials like *miec* (mixed ionic and electronic conductors) could obviate to this problem.

3.4 Parametric analysis

Having verified the validity of the model, it is now possible to use it to predict how changing certain parameters would influence the performance of the cell, in order to focus on the most relevant aspects when designing new materials and configurations. Several aspects will be investigated:

- Operating conditions: temperature, gas inlet velocity, fuel gas composition;
- Variations in the materials or geometry of the cell (conductivity, kinetic parameters, thickness of the active layers, porosity).

3.4.1 Temperature

The model has been operated at the temperatures of 750, 800 and 850°C (with 800 being the base case), and all other parameters maintained constant. The effect can be seen in Figure 3.6.

As can be expected, increasing temperature also increases the performance of the cell, since it promotes most of the processes in the cell: kinetics, matter transport via diffusion, and ionic conduction. However, this is not true at low current densities: the OCV is actually higher at lower temperature, according to Nernst's equation, and for i < 1500 A/m^2, low temperatures are preferred. Given the results of figure 3.5, though, it is advantageous to operate at much higher current densities than that, so the generalization that increasing temperature also increases cell performance is justified. There is an engineering limit to the operating temperature, although the model does not represent it: fuel cells are particularly subjected to degradation of properties over time, and while higher temperatures lead to a more efficient power

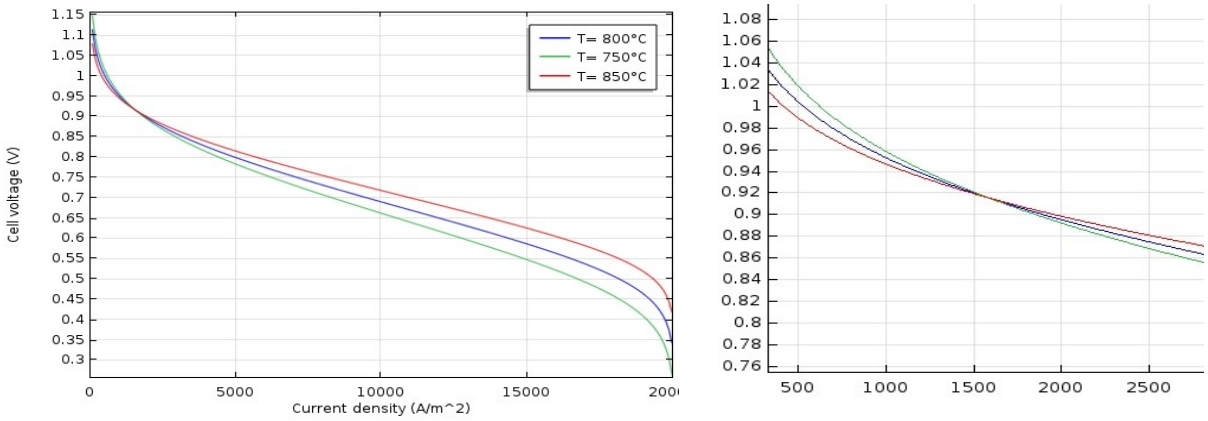

a) *b)*

Figure 3.6. *a) Polarization curves parametric in the temperature. b) Magnification of the zone where the curves cross each other.*

output, they also reduce the lifespan of the cells considerably [38].

One final consideration regards the validity of the assumption of uniform temperature inside the cell. Experimental investigations of temperature gradients inside the cell lead to difference of less than 20°C [28]. Considering that for a reasonable value of current density, 15000 A/m^2, increasing or decreasing temperature by 50°C changes the value of the potential by less than 7%, this means that the temperature gradients that can be expected inside the cell do not significantly affect the results.

3.4.2 Inlet velocity

Instead of changing the inlet velocity in only one of the channels, the ratio v_a / v_c has been maintained constant, so that only transport phenomena are affected by a different flow rate value. As said in Chapter 2, the inlet velocities in the anode and cathode channel of the commercial cell considered are 1.617 and 3.639 m/s respectively, corresponding to volumetric flow rates of 8 and 10 NL/min. These values have been multiplied by 0.75 and 0.5, the resulting polarization curves are reported in Figure 3.7.

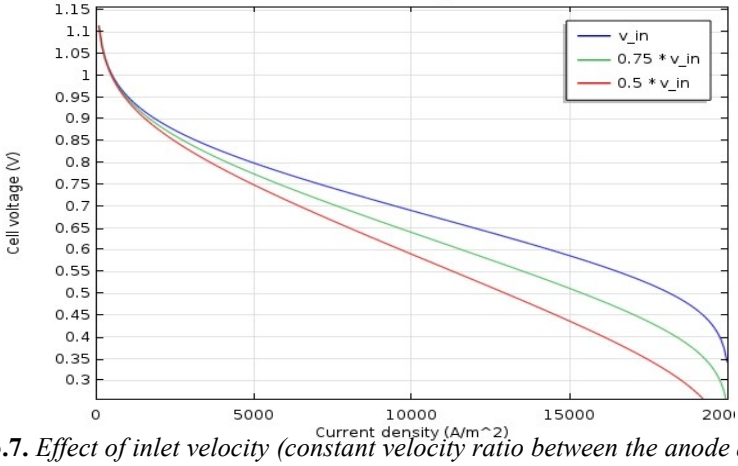

Figure 3.7. *Effect of inlet velocity (constant velocity ratio between the anode and the cathode channel) on the polarization curve.*

Reducing gas velocities reduces the performance of the cell considerably. This is due to the reduced feed of reactants: at a given *i*, (i.e. given consumption rates), the molar fractions of hydrogen and oxygen at the TPB decrease, which in turn leads to larger concentration overpotentials (as can be seen from Eqs. 2.23 and 2.26).

In this analysis, the molar ration between oxygen and hydrogen flow rates has been kept constant, at $r_{O2/H2} = 0.272$. Next, the effect of changing the air flow rate while keeping the fuel flow rate constant has been examined. This means that there will be a contribution due to velocity, and one to different oxygen/hydrogen ratio, although the effect of velocity has already been evaluated. This is the only way to evaluate different species ratios, since for economic reasons enriched air is never used in fuel cells. Despite being the value for which polarization data were available, it is unusual to have a molar ratio lower than 0.5 (which would be the stoichiometric value), and cells are usually operated with an excess of air, since there is an economic value in recovering unreacted hydrogen, while this is not true for unreacted oxygen [1]. In this simulation, the fuel flow rate has been maintained constant at 8 NL/min, while the air flow rate has been set at 10 (base case), 20 and 30 NL/min, corresponding to oxygen-to-hydrogen ratios of 0.272, 0.544 and 0.816 respectively. It is worth noticing that even the higher value does not influence the flow regime, since Re < 200. Results are reported in Figure 3.8.

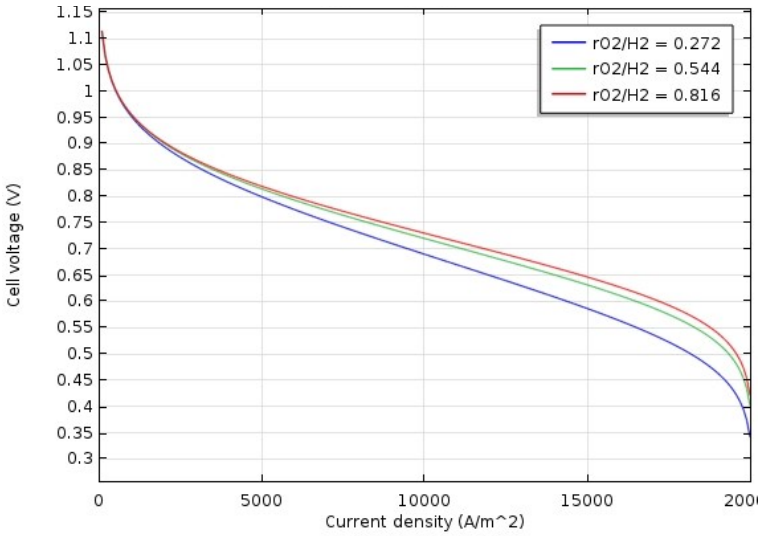

Figure 3.8. *Effect of increased oxygen-to-hydrogen ratio.*

At any given current density, V_{cell} increases as $r_{O2/H2}$ increases, for the same reason that in Fig. 3.7 lowering the inlet velocities lowered the polarization curve: because increasing bulk velocity reduces concentration overpotentials, and while in this latter case this only applies to the cathode side, the effect is still noticeable, although not as impactful as varying the velocity on both sides. Over a $r_{O2/H2}$ value of 0.5, however, the gain is minimal, because oxygen concentration tends to become more uniform in the cathode (hydrogen is the limiting reactant). This means that beyond a certain value, when concentration

overpotentials at the anode are minimized, the air flow rate does not influence the cell performance anymore, and can therefore be used to control the temperature in the system [42].

3.4.3 Fraction of steam in the fuel side

The effect of a higher molar fraction of water in the fuel feed has been analyzed. The predicted behavior is that lowering the molar fraction of hydrogen in the feed would decrease the effectiveness of the cell, because it would lower the OCV according to the Nernst equation (Eq. 2.28). For this simulation, the hydrogen molar fraction has been set to 0.965 (base case), 0.9 and 0.85, while maintaining the other operating conditions (including the fuel flow rate). Results are shown in Figure 3.9.

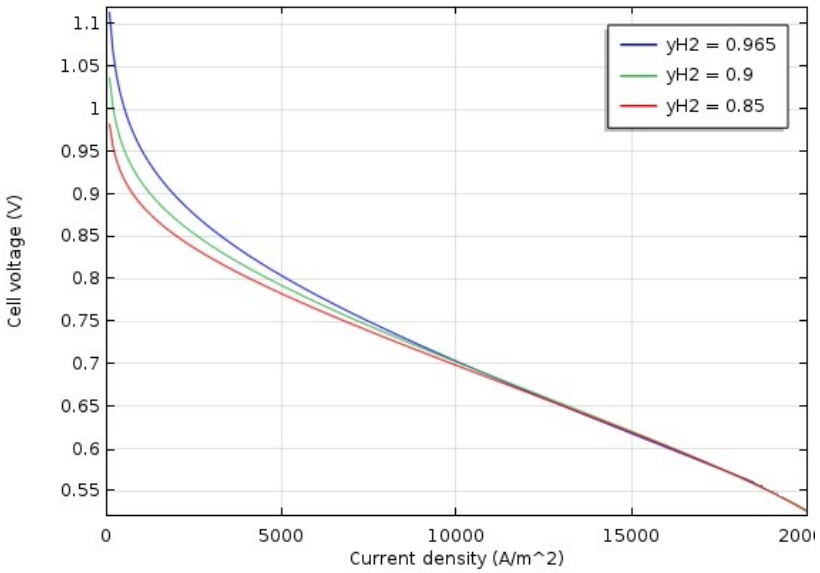

Figure 3.9. *Effect of water vapor in the fuel feed.*

As expected, the OCV is lower at lower hydrogen molar fractions in the feed. However, the gap decreases at higher current density values. There are two factors that contribute to this behavior. First, Eq. 2.21 predicts that a decrease in the molar fraction of hydrogen will decrease i_{0a}, which reduces the anode overpotential at a given current density. Second, a lower hydrogen molar fraction reduces the absolute value of the equilibrium potential step in Eq. 2.23, further reducing η_a. This agrees with previous research into Ni/YSZ electrodes: some groups [43, 44] have experimentally proven the catalytic effect of water on the kinetic rate of hydrogen oxidation, while others [45, 46] have focused on concentration effects. Since the model is able to reproduce such behavior, this further attests the validity of the description of electrochemical and physical processes.

3.4.4 Ionic conductivities

Using materials different from those considered in the model influences several parameters, from gas transport via diffusion (different porosity and tortuosity), to the reaction kinetics (the kinetic expressions used were valid exclusively for Ni/YSZ and LSM/YSZ electrodes) to the electronic and ionic conduction. However, it may be helpful to see the contribution that material properties give to the total polarization curve.

Varying the conductivity of the materials is a first step in doing so. First, only the results for ionic conductivities are reported: the resistance to the transfer of oxygen ions is 4 to 5 orders of magnitude greater than the electronic resistance, and varying the latter does not change the polarization curve in any appreciable way. Second, this analysis does not consider other properties that are likely to change with the use of different materials, which will be investigated in the following paragraphs.

The value for ionic conductivity has been set to half and twice the base case value for each layer (functional anode, cathode, electrolyte). Ionic conductivities are also a function of temperature, but this variable has been kept constant in this analysis. Results are reported in Figure 3.10.

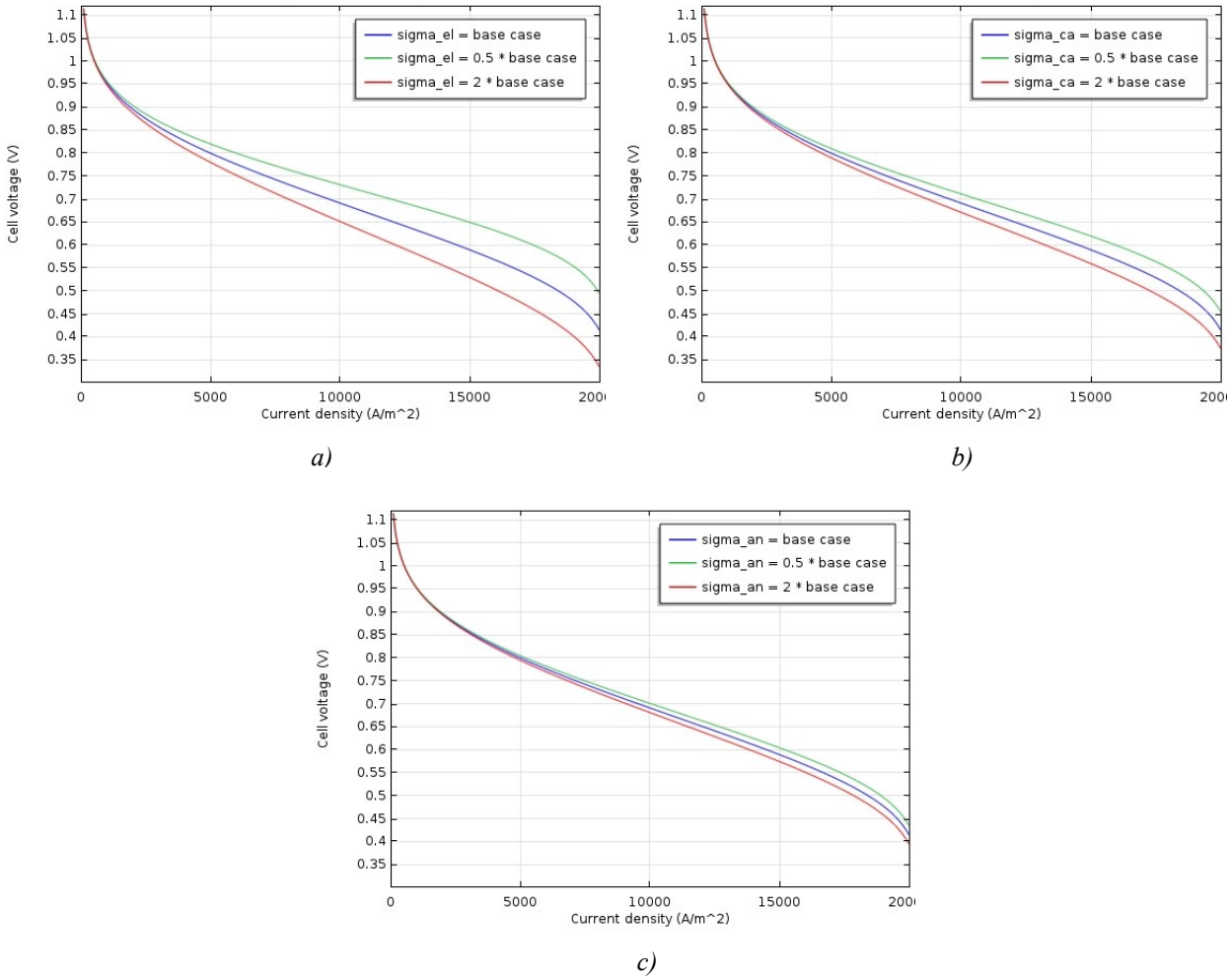

Figure 3.10. *Effect of ionic conductivity of the electrolyte (a), cathode (b) and anode (c) layers.*

The most relevant effect is associated with a variation in conductivity in the electrolyte layer. This is likely because the dense electrolyte phase is the most important contribution to ohmic overpotential. Furthermore, the reactions occur inside the electrodes, so the ions do not generally have to migrate through the whole thickness of the ion-conducting phase, while they do have to cross the entire section of the electrolyte.

3.4.5 Kinetic parameters

In the previous paragraph the effect of ionic conductivity has been considered, this paragraph will explore the effect of kinetic parameters. Different materials will have different kinetics for the electrochemical reactions taking place inside the electrodes. It is worthwhile to investigate the effect of the reaction kinetics on the overall performance, so that research on new materials can focus on the most relevant aspect to improve the power output. In particular, the reference exchange currents per unit of TPB length, used in Eqs 2.21 and 2.25 for the anode and cathode reaction respectively, will be increased, leading to faster reaction rates. Results are reported in Figure 3.11.

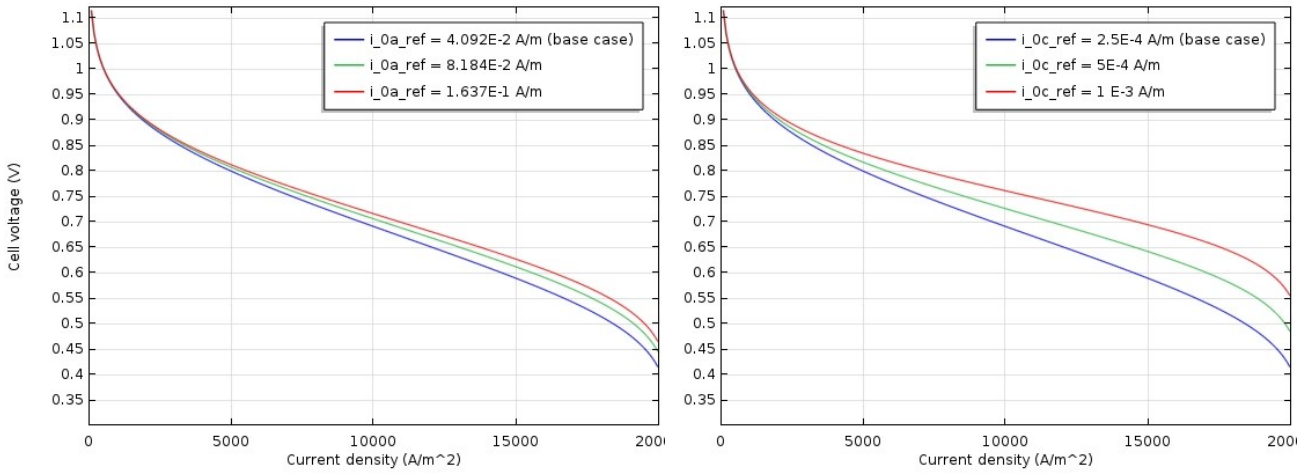

a) *b)*

Figure 3.11. *Effect of reference exchange current per unit of TPB length, for the hydrogen oxidation reaction (a) and the oxygen reduction reaction (b).*

The first consideration that can be drawn from this analysis is that the cathode kinetics influence the overall performance of the cell in the most relevant way, as was to be expected since the oxygen reduction reaction is the slowest one. Another consideration is that improving anode kinetics has diminishing returns, which is consistent with the oxygen reduction reaction being the limiting step.
This result means that, in researching new materials, it can be a good trade-off to have lower ionic conductivity at the cathode in exchange for faster oxygen reduction kinetics.

3.4.6 Layers thickness

Material properties are not the only non-operating condition that influences the performance of the cell. The geometry used in the study reflects a commercial cell that uses very well known materials for the electrodes, but when researching into new materials, it becomes important to optimize the constructive parameters of the cell in which they are to be used as well. In this paragraph, the effect of anode and cathode thickness will be investigated. The effect of the electrolyte thickness can be immediately understood without a simulation, and was not considered: the electrolyte should be as thin as possible to minimize ohmic resistances (as seen in paragraph 3.4.4, this contributes to the ohmic overpotential more than the electrodes do), the lower limit being purely technological in nature (ensuring gas sealing and electrical insulation with as thin a layer as can be reliably manufactured).

In this analysis, the thickness of the cathode and the functional layer of the anode has been multiplied and divided by a factor of 2 (in the base case, the anode is 12 μm thick, and the cathode 10 μm). Results are presented in Figure 3.12.

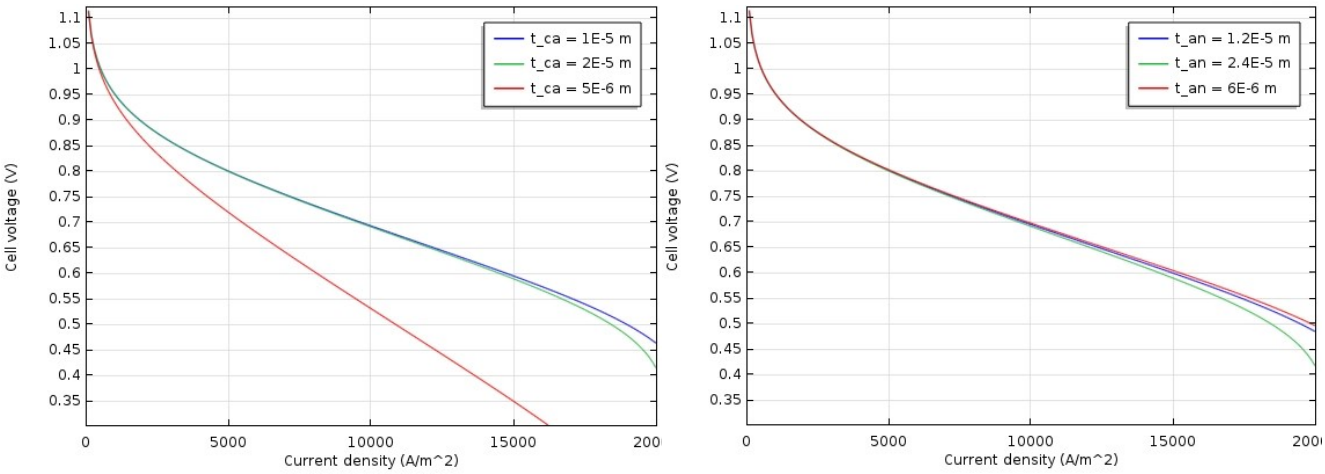

a) *b)*

Figure 3.12. *Effect of changing the thickness of the cathode (a) and the anode (b).*

In order to interpret these results, the actual active thickness of the electrode has to be considered. Fig. 3.12*a* shows that reducing the cathode thickness severely reduces the output of the cell, because it reduces the active sites for the reaction. Following this result, one might expect that increasing the thickness will improve the performance, while the simulation shows the opposite. That is due to the fact that the reaction is localized near the cathode – electrolyte boundary, the active area is thinner than the actual electrode, and therefore increasing its thickness does not increase reaction rate. If anything, it introduces a small resistance to diffusion, that increases the concentration overpotential at higher current densities.

Fig 3.12*b* shows a different behavior for the anode. Here, increasing the thickness introduces more concentration overpotential as was to be expected, while reducing the thickness does not reduce the cell performance, it actually increases it very slightly (especially at high current densities, this is again due

to the lower concentration overpotential). This means that the active part of the anode is much thinner than the electrode itself, and so reducing the thickness does not reduce the active sites for the reaction, because those are located in the region closer to the electrolyte. This has been further confirmed by studies focused on experimentally identified microstructural characteristics [22]. Further reducing the thickness so that it is smaller than the active area would lead to a severe reduction in effectiveness as was seen for the cathode.

Since the active part of the anode is much thinner than the electrode itself, the assumption that the reaction only takes place in the functional part of the anode and not in the structural layer, despite the two being made of the same material, is justified.

3.4.7 Porosity

At first glance, porosity should not be an interesting parameter to investigate, since it is clear that decreasing porosity would increase the concentration overpotential due to smaller diffusion coefficients (the diffusion coefficients are correlated to the porosity, to account for diffusion in a porous medium rather than free diffusion). However, this does not consider that decreasing porosity means having a stronger sintering degree, which in turn means an increase in the contact angle and the properties associated with it (length of TPB per unit volume, effective conductivity factors), as well as having lower permeabilities in the porous matrixes. Therefore, a decrease in porosity is associated with negative effects on the performance (resistance to diffusion, lower permeabilities), as well as positive ones (better conductivities, more active sites).

This makes porosity a parameter whose effect cannot immediately be identified, not even qualitatively. Unfortunately, the relations between the porosity and the parameters that are, directly or indirectly, dependent on it, require a detailed analysis of the microstructure of the electrodes, that is beyond the scope of this study.

Effective diffusion coefficients are the only parameter that have an explicit relation to the porosity. For all other quantities, very rough estimates can be made with dimensional analysis. Porosity, despite being a dimensionless quantity, is a ratio of volumes. The length of TPB should, at least as an order of magnitude, scale with exponent 1/3 with respect to porosity. Permeability should scale with exponent 2/3, and so do conductivity factors, since they are related to the cross-sectional areas of contact between particles. Bear in mind, once again, that these are just estimates, and the effective parameters in a sintered porous media with a different degree of porosity are bound to have much more complex relations.

In Figure 3.13, the effect of decreased porosity in the cathode and the anode functional layer have been investigated, varying all other parameters related to porosity with the estimates detailed above. For both electrodes, the positive effect of a higher sintering degree is countered by the added concentration overpotential and the lower permeability, although the decrease in performance is smaller at the cathode

since it is more influenced by an increase in effective ionic conductivity. Therefore, lowering porosity does not lead to more efficient cells.

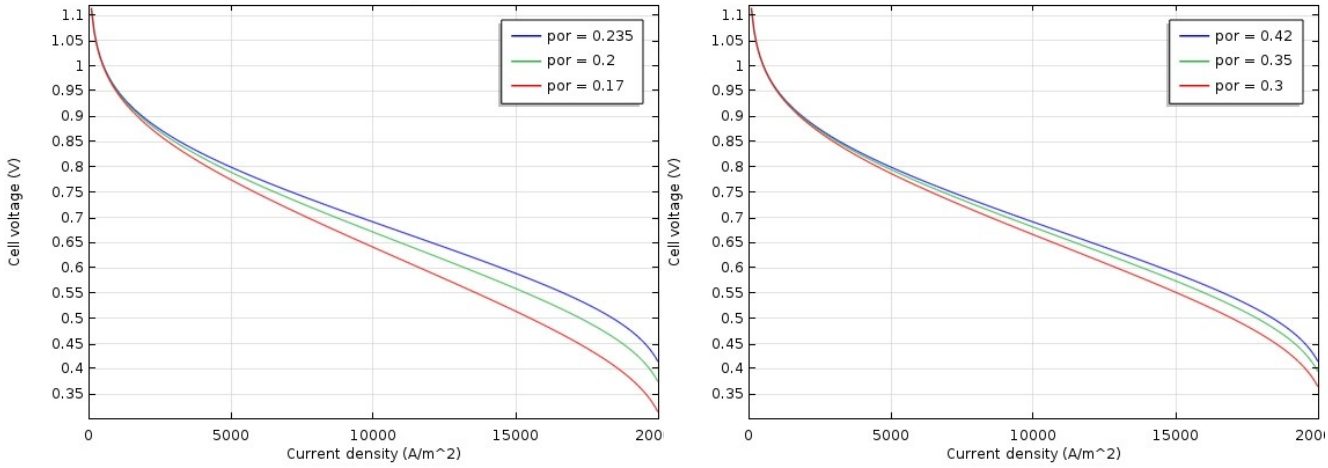

a) *b)*

Figure 3.13. *Effect of the porosity at the anode (a) and cathode (b). All other parameters related to porosity or sintering degree have been scaled accordingly, using dimensional analysis as a very rough estimation.*

There is, however, a way to get the benefits of a higher sintering degree without the disadvantages of it. Adding pore-formers to the powder before sintering (organic compounds that completely decompose into gaseous products under the high sintering temperatures) can result in larger contact angles, therefore improving the TPB length and the effective conductivity, without increasing porosity. The use of pore-formers would even lead to larger pores, and consequently a lower tortuosity factor [47] (which is not a parameter of this model, but is one of the variables upon which the permeability is dependent), therefore slightly improving gas diffusion, resulting in lower concentration overpotentials (although this last effect is likely negligible, compared to the other benefits of a larger contact angle between particles).

Chapter 4

Electrochemical impedance spectroscopy

In the previous chapter, polarization curves were analyzed. While this approach allows for the identification of the optimal constructive and operating parameters, it does not isolate the physical processes responsible for a variation in the performance. Electrochemical impedance spectroscopy (EIS) can be a very useful too in that regard, because its results are directly related to the characteristic times of the phenomena occurring inside the system, and can therefore be used to identify how changing certain parameters influences the physical processes. Much like in Chapter 3, first the technique will be described in detail, and then it will be used to evaluate the effect of varying material and geometrical properties.

4.1 EIS and Nyquist plots

The basics for EIS were covered in paragraph 1.4.1, here some more details will be added in order to better interpret the simulated results.

EIS consists in adding small oscillations around a fixed value to the system input, and recording the output. Processes with characteristic times much larger than the oscillation period will not be affected by it, and only react to the base value, while faster processes will lead to an oscillating output that is out of phase with the input. Since impedance is a complex number, the imaginary *vs.* the real part can be represented. This gives a single point on a Cartesian plane, that can be connected to the origin forming a vector whose length is the module of the impedance (which is the analogous of the resistance for oscillating inputs), and whose angle with the abscissae axis is the phase shift. This is called a Nyquist plot (Figure 4.1).

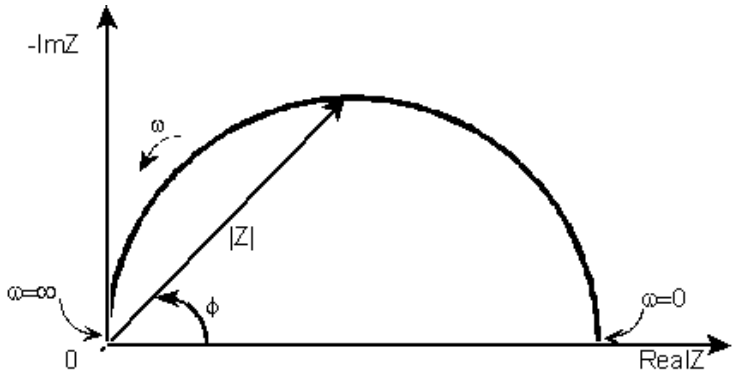

Figure 4.1. *Nyquist plot (imaginary vs. real part of the impedance). This is not actually a curve, but a collection of points, each associated with a given frequency.*

Each frequency corresponds to a single point on the plot, the Nyquist plot is a sum of points, each associated with a particular frequency (although a major shortcoming of this type of plot is that it is not immediately clear what frequency corresponds to a certain point). The module of the impedance falls as the frequency rises (in fuel cells, not in all circuits: the Nyquist plot can be used to analyze a wide variety of electrical and electrochemical processes, and even control systems and signal processing), and therefore the lower frequencies are on the right side, and the higher frequencies on the left one.
Note that the ordinates axis reports the opposite of the imaginary part of the impedance: this is because it is a negative value, but it is conventionally plotted in the first quadrant. This notation will be used in all Nyquist plots produced by the model (Fig. 4.3 – 4.10).
In this study, the frequency has been varied between 0.1 and 10^4 Hz with an exponential growth, spanning a total of 50 data points. COMSOL uses a particular type of study step, the Frequency-Domain, Perturbation study, to simulate a sinusoidal input of given amplitude around a base value (for stability reasons, it is helpful to apply the perturbation to a solution for the steady-state study).
One parameter that has not been introduced earlier in this thesis, but which is important for simulating the behavior of the cell under perturbations, is the double layer capacitance. At the interface between electrodes and the electrolyte, there is a local accumulation of charge, which acts as a capacitor (Figure 4.2). While in steady – state conditions this does not influence the results, it becomes relevant for EIS analysis.

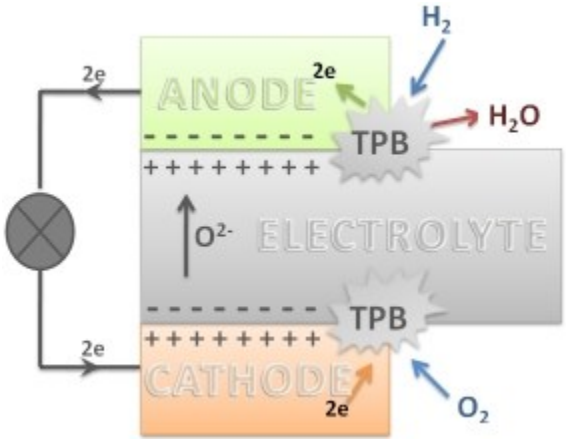

Figure 4.2. *Representation of charge accumulation at the electrode-electrolyte interface, creating a double layer capacitance.*

The effect of double layer capacitance can be evaluated by the COMSOL model. However, the values of the specific capacitances for the two electrodes are not easy to obtain, especially since they depend on many factors including electrode potential, temperature, species concentration, contact area between the layers, etc. One way to obtain the value for the capacitance in SOFCs is through Raman or infrared spectroscopy [48, 49], but such analysis should be conducted for every operating condition which will

be varied in this study, and no literature data exist for the exact conditions and the different values at which the parameters will be set.

However, the goal of this chapter is to analyze how varying certain parameters influences the processes taking place inside the cell. The values of the specific capacities is not relevant to this, and can be set at a reasonable value, according to literature data, of 150 F/m^2 for both electrodes. The resulting Nyquist plot is reported in Figure 4.3. If anything, the double layer capacitance can be an obstacle, superimposing its effect to those of other phenomena that are worth investigating. In this particular case this is not a problem since the arcs are already neatly separated, but for other systems a possible solution would be to arbitrarily increase the value of the specific capacity in order to artificially separate the arc. This would allow to discern the effect that a change in parameters has on those arcs.

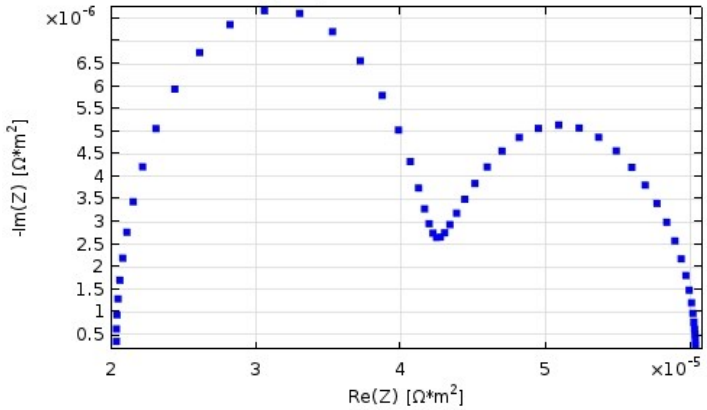

Figure 4.3. *Nyquist plot for the system at base case conditions for c_{dl} = 150 F/m^2.*

The Nyquist plot reported in Fig. 4.3 is qualitatively similar to that obtained for a Forschungszentrum Jülich anode supported single cell operated in similar (though not identical) conditions. An exact match is not the goal of this study, which rather focuses on the identification of the phenomena occurring inside the cell and their characteristic times.

4.2 Phenomena associated with the arcs

Figure 4.3 shows the presence of two distinct arcs in the Nyquist plot. First, it is useful to understand to what type of phenomena those arcs are associated with. Given that frequency increases going from right to left, and that the effect of higher frequencies is only perceived by faster processes, it is clear that the right curve is associated with slow processes and the left curve to fast ones. What is left to determine is exactly which, among the phenomena taking place inside the cell (electrochemical reactions, electronic and ionic conduction, gas diffusion), can be considered slow or fast.

A first test will be how a higher potential influences the results. The OCV for the cell at base case conditions is 1.142 *V*, the cell has also been simulated at 1.2 and 1.3 *V*. Results are presented in Figure 4.4. As potential increases, the impedance of the cell decreases for any given frequency. However, the left arc is mainly affected, while the right arc remains substantially unchanged. Therefore, the right arc must represent phenomena that are unrelated to the applied potential. Since reaction rates depend on the

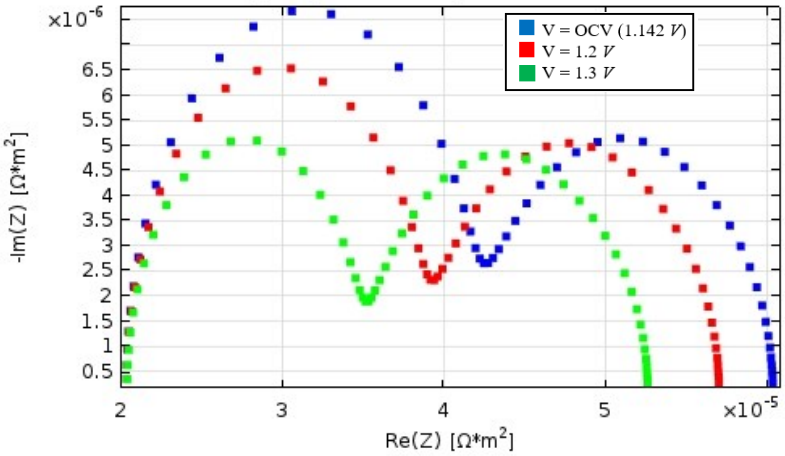

Figure 4.4. *Effect of increased applied potential.*

potential, and so do the electronic and ionic conductions, a tentative explanations is that the right arc represents the other steps, the diffusion of gases. One way to test this hypothesis is to arbitrarily decrease diffusion coefficients, to see if this affects the right arc. An effect on the left arc is expected as well, since increasing resistance to diffusion also increases concentration overpotential, and therefore lowers the exchange current for a given applied potential. A Nyquist plot in which diffusion coefficients have been arbitrarily decreased by a factor of 10 is presented in Figure 4.5.

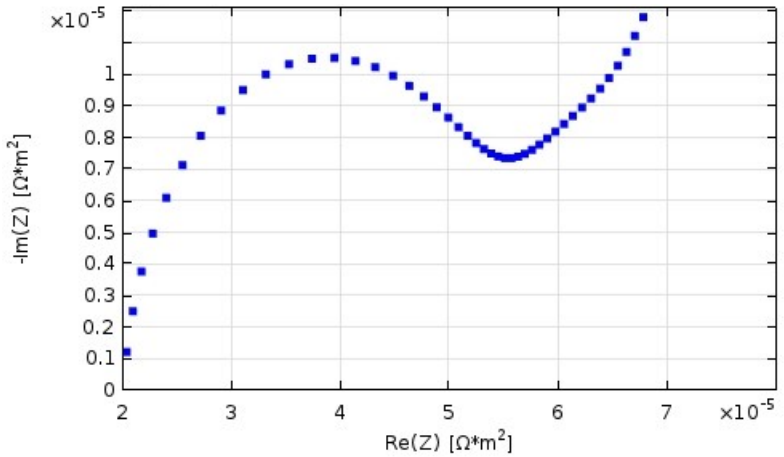

Figure 4.5. *Nyquist plot with arbitrarily reduced diffusion coefficients on the two sides.*

As predicted, the left arc has expanded because slower diffusion greatly increases concentration overpotential. The right arc, however, is not recognizable anymore, and diverges, in accord to the behavior known in systems under diffusive control (mass transfer or Warburg impedance). This is a further proof that the interpretative hypothesis was correct, and the right arc is associated with diffusive processes.

4.3 Parametric analysis

Several simulations have been carried out to identify how certain parameters influence the spectra, and therefore the phenomena that those spectra identify. This analysis is similar to what was conducted in paragraph 3.4, but instead of analyzing the performance of the cell, the effect of a number of parameters on the processes taking place inside the cell has been evaluated under perturbations, resulting in Nyquist plots.

4.3.1 Temperature

Many of the model's parameters depend on temperature. The overall effect of temperature on the module of the impedance is fairly straightforward to predict, since it has already been established that an increase in temperature dramatically improves the performance, and so would lead to lower resistances (i.e. impedance). The expected result is that at high temperature the arcs would be both shifted to the left and reduced in height. It is however interesting to see how the two arcs react to different temperatures. Results of the simulation, with T = 750°C, 800 °C (base case) and 850°C, are reported in Figure 4.6.

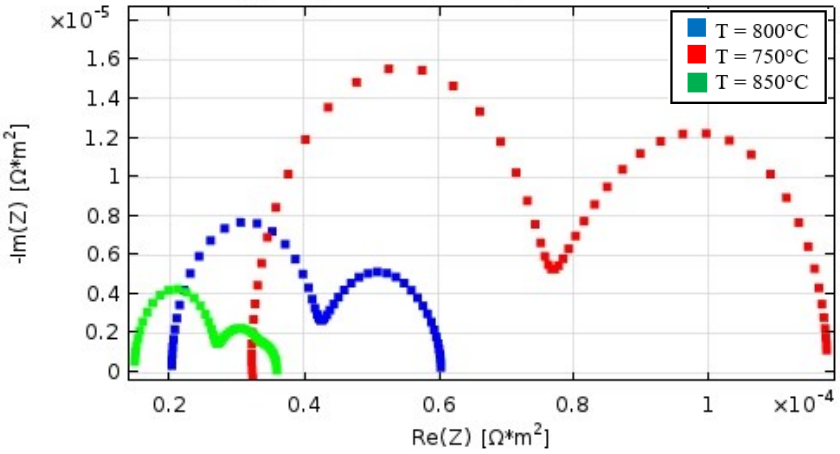

Figure 4.6. *Effect of system temperature on the Nyquist plot.*

While both arcs are reduced in size, the ratio between them is not constant. The lower the temperature, the more relevant the resistances associated with diffusion become. This means that, while an increase in temperature has a positive effect on reaction kinetics and electronic and ionic conduction, it has an even greater effect on the diffusion of gases in and out of the electrodes. This is a result that was not immediately identifiable by looking at steady-state simulations.
Another interesting aspect is that at high temperature the right arc seems to be the superposition of two distinct arcs. Simulations at higher temperature accentuate this aspect. This is likely due to the contributions to a different diffusion resistance of the anode and the cathode channel.

4.3.2 Fraction of steam in the fuel side

The expected behavior of a decrease in hydrogen molar fraction is a reduction of the left arc due to a lower OCV (Eq. 2.28), and a larger effect on the right arc because of smaller gradients and therefore slower diffusion processes. The hydrogen molar fraction has been set to 0.965 (base case), 0.9 and 0.85, simulation results are reported in Figure 4.7.

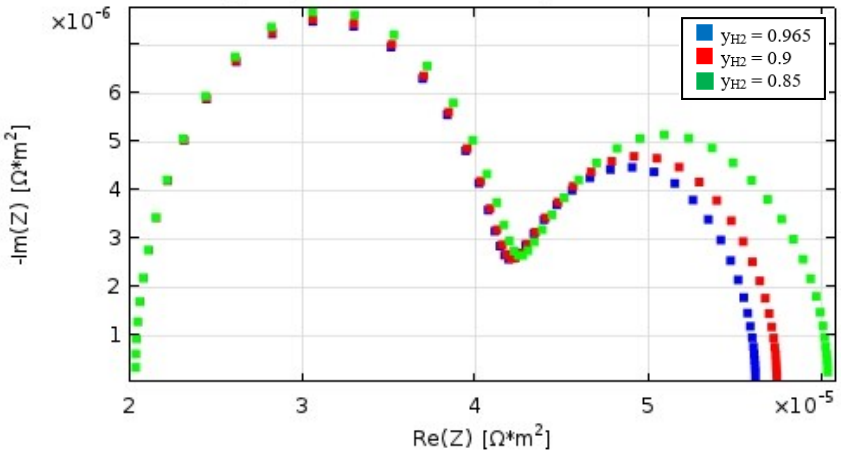

Figure 4.7. *Effect of hydrogen molar fraction in the fuel feed on the Nyquist plot.*

The effect on the left arc, corresponding to the electrochemical processes, is less pronounced than expected. While a lower OCV depresses the effectiveness of the cell, a lower hydrogen molar fraction also causes a reduction in the exchange current at the anode (Eq. 2.21), reducing concentration overpotentials. Furthermore, the anodic activation overpotential is reduced as well (Eq. 2.23). These two beneficial effects partly counterbalance the effect on the OCV, and the increase in impedance module is almost exclusively due to the slower phenomena, i.e. the diffusion of gaseous species.

4.3.3 Ionic conductivities

The effect of different ionic conductivities has been investigated. This can be due to different materials used, or different sintering degrees, since for the electrodes effective conductivities are not inherent properties, but depend on how the electrode was manufactured. The simulation has also been conducted varying the electronic conductivities, but since those are several orders of magnitude greater than ionic ones, no effect was observed on the Nyquist plot, and results are not reported here.

Since conduction is an electrochemical phenomenon, the expected behavior is a contraction of the arc corresponding to faster processes, without influencing the diffusion. Simulations have been conducted for the ionic conductivity at the anode, at the cathode and in the electrolyte. In all cases, the base case values have been halved and doubled. Results are reported in Figure 4.8.

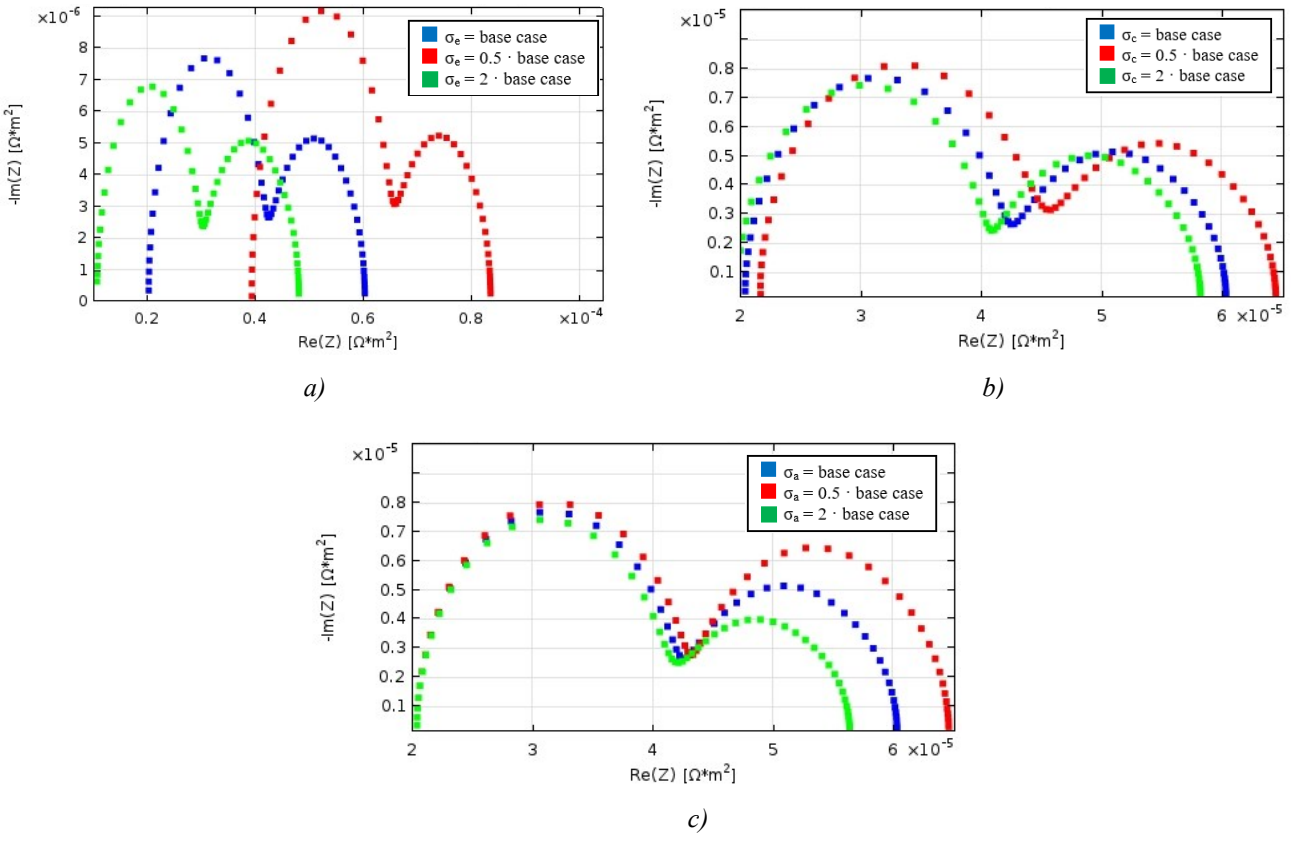

Figure 4.8. *Nyquist plots with the effect of ionic conductivity of the electrolyte (a), cathode (b), and anode (c).*

Fig. 4.8*a* shows that only electrochemical phenomena are affected by a variation in the ionic conductivity of the electrolyte layer, with virtually no effect on the diffusion arc, as was expected. In a Nyquist plot, ohmic resistance is represented by the intersection of the curve with the abscissae axis, which corresponds to the point at the lowest frequency. Increasing conductivity shifts the plot to the left, which is consistent with a decrease in ohmic resistance.

A similar situation is seen in Fig 4.8*b*, although in this case a very small contraction of the diffusion arc can be seen. This is likely due to the fact that increasing conductivity removes oxygen ions from the reaction site faster, which leads to a greater concentration gradient that promotes diffusion. The effect is minimal because on the cathode side the gases have to diffuse through a very thin layer (the thickness of the cathode plus the current collector is only 70 μm).
This interpretation is further confirmed by the results in Fig 4.8*c*. Here the reduced resistance due to electrochemical phenomena is accompanied by a very noticeable effect on the diffusion arc as well. Bringing oxygen ions to the reaction sites faster creates a higher concentration gradient like in the cathode. However, unlike the cathode, at the anode the thickness is much more relevant, since the anodic supporting layer is 1.5 mm thick. Higher concentration gradients have the same beneficial effect that they have in the cathode, however the resistance associated with diffusion is dominated by what happens in the anode side, and improving this process has a much more noticeable effect compared to the cathode side.
This is one of the limits of EIS: while it is very helpful in identifying the relative speed of the processes occurring inside the cell and how they influence each other, processes with the similar characteristic times are lumped together, and their effect correspond to a single curve that is the superposition of the individual resistances. Separating these effects is not always easy: as explained in 4.1, sometimes the double layer capacitance can be used to artificially separate arcs (only in models, not in experimental observations); other times, extreme conditions can de-couple the arcs, when they change the characteristic times of the phenomena. In general, though, singling out individual processes rather than group of processes with similar characteristic times can be challenging.

4.3.4 Kinetic parameters

Changing kinetic parameters should influence the left arc, but as seen in the previous paragraph, faster reactions induce larger concentration gradients that modify the shape of the diffusion arcs as well. The effect should be more noticeable on the anode side, because of the large thickness that makes it the dominant contribution. For this simulation, the reference exchange current per unit of TPB length has been halved and doubled on each side. Figure 4.9 shows the results of the simulation.
On the anode side (Fig. 4.9*a*), the concentration gradients greatly accelerate the diffusion at faster reaction rates. The effect on electrochemical processes, however, is not so relevant. The opposite situation can be seen on the cathode side (Fig 4.9*b*). Here the reduced electrode thickness makes diffusive processes almost independent on reaction rates, while faster reactions heavily influence the electrochemical arc, since the oxygen reduction reaction is the limiting step.
It is worth remembering that having the two arcs similar size (like the red curve in Fig 4.9*a*, or the green one in Fig. 4.9*b*) does not mean that the electrochemical and diffusive phenomena contribute equally to

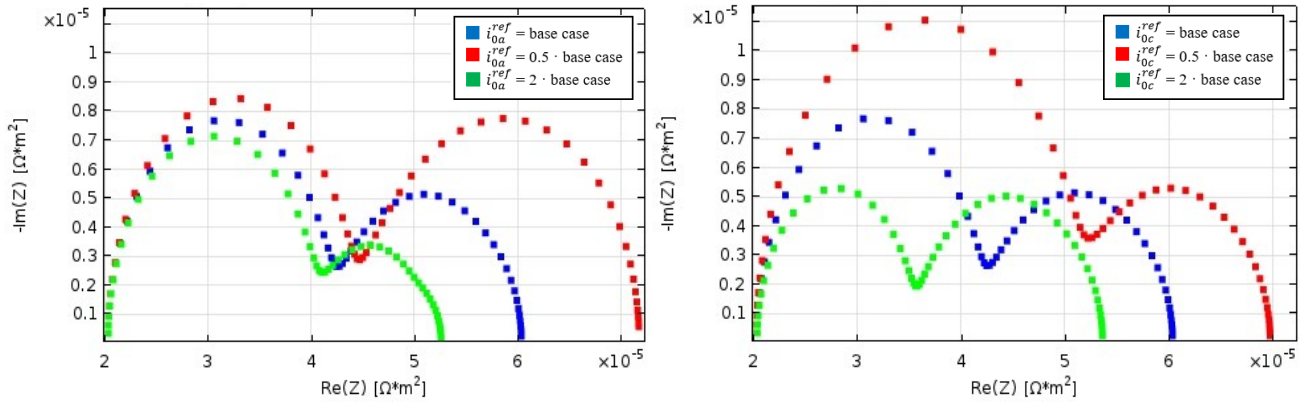

a) *b)*

Figure 4.9. *Effect of anode (a) and cathode (b) exchange current densities on the Nyquist plot.*

the total resistance of the system. It is a common mistake to assume that the size of the arcs are proportional to the contributions of the processes they represent. In reality, the module of the impedance (which is the analogous to the resistance for oscillating regimes) is the distance of a single frequency point from the origin. The goal of the analysis conducted in this chapter is to identify the effect of parameters changes on the phenomena occurring inside the cell, not to quantify their contributions.

4.3.5 Electrodes thickness

In paragraph 3.4.6 the effect of electrode thickness on performance has been evaluated. Based on those results, the expected behavior is a small reduction in diffusion resistance as the thickness decreases, until the thickness becomes smaller than the active part of the electrode, at which point the reduction in reaction sites should severely increase the resistance. The effect of an increase in thickness is fairly straightforward, a thicker electrode does not increase performances since the base case thickness is already larger than the active area for both electrodes, it only slightly increases resistance to diffusion, and therefore these results are not reported here. For this simulation, the thickness has been reduced by 75%, 50% and 25% of the base case value (12 µm for the anode, 10 µm for the cathode). Results are reported in Figure 4.10.

Reducing the thickness of the anode (Fig. 4.10*a*) has almost no effect until a certain threshold is reached, at which point the electrode is thinner than the active layer required for the reaction, and this reduces the effectiveness greatly. At the cathode (Fig. 4.10*b*) the active layer falls just barely within the base case thickness, and any reduction in the electrode's dimension reduces performances. The effect on the diffusion arc is once again related to the thickness of the porous matrix that the gas has to diffuse through to reach the active sites: for the anode, the concentration gradients induced by slower reaction rates

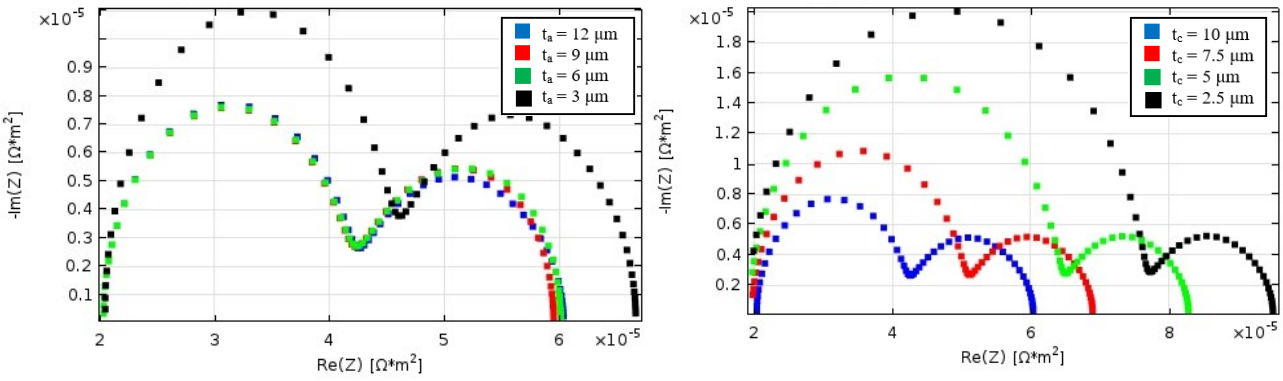

a) *b)*

Figure 4.10. *Effect of decreasing electrode thickness at the anode (a) and cathode (d) on the Nyquist plot.*

influence the diffusion resistance in an appreciable way, whereas at the cathode side the porous phase is very thin and the effect of concentration gradients is barely noticeable.

Conclusions

The goal of this study has been the development of a tool that could be used to characterize and optimize cell geometry an operating conditions in new generations of solid oxide fuel cells, as well as help identifying what properties new materials should have in order to maximize their efficiency. In particular, there is an ongoing collaboration between the Industrial Engineering department and the department of Chemical Sciences at the University of Padua, aimed at developing new materials for SOFCs that can be active at lower temperatures, as well as using those materials in working prototypes.

The tool developed is a mathematical model for SOFCs, which has been created using COMSOL Multiphysics, a commercially available finite element simulator. The model solves gas flow, ions and electrons field in every part of the cell, including solid domains. The model has been applied to a well known and studied existing SOFC, so that kinetics, material properties, geometry and microstructural information were readily available, as well as experimental data with which to test its effectiveness.

Subsequently, the model has been tested against said experimental data, without any adjustable parameters, and has been found to adequately represent the different processes inside the cell. Once its validity has been verified, the model has been used to evaluate the effect of changing parameters, in order to analyze the contribution that such changes give to the overall performance. The parameters whose effect has been evaluated are temperature, inlet velocities (both with fixed and different ratios in the two channels), fuel composition, ionic conductivities in the electrodes and the electrolyte, kinetic parameters for both global reactions, electrode thicknesses and porosities. Some of these parameters are purely operating, some are related to cell geometry, while others pertain exclusively to the materials used, so that when trade-offs in intrinsic properties have to be considered while developing new materials, there can be an informed choice about the most effective set of properties.

Two types of simulations have been conducted with changing parameters. First, the model has been run under steady-state conditions, obtaining a simulated polarization curve that allows to evaluate the effect that parameter changes have on global effectiveness. Then, it has been used to simulate the results of an electrochemical diagnostic tool, EIS (electrochemical impedance spectroscopy), that uses oscillating inputs to analyze the characteristic times of the phenomena inside the cell, allowing to break down their contributions. Generally, when EIS is applied experimentally, the behavior of the system is confronted with equivalent circuits whose parameters are fitted on the results, assigning each circuit element to a particular process, whereas this model generates a Nyquist plot (one of the outputs for EIS) directly from the response of the real cell, simulated with its actual processes, therefore removing the need for analogies with equivalent circuits.

Among the interesting results that could help maximize the performance of future prototypes, there are:

- After a certain point increasing air flow rate does not improve cell performance anymore, and can therefore be used to control the system temperature;
- More diluted fuel streams do not negatively affect performances at high current densities;
- Good cathode materials, both in terms of ionic conductivity and catalytic properties, contribute more than good anode materials to the performance of the cell, confirming that oxygen reduction is one of the critical steps;
- The active part of the electrodes can be smaller than the thickness of the electrode. The simulation can help identifying an optimal thickness that reduces resistances due to gas diffusion without compromising the number of active sites;
- A higher degree of compenetration between sintered particles in the electrodes will increase performance, but only as long as the same porosity is maintained with the use of pore-formers. Higher sintering degrees without pore-formers result in lower porosity which in turn depresses efficiency;
- For anode-supported cells, improvements on the cathode sides are more associated with electrochemical phenomena, while on the anode side diffusion resistances are the leading sources of potential losses.

Future developments concern using this model to obtain unknown properties and to optimize cell prototypes: now that it has been proven to accurately represent the physical processes occurring inside a fuel cell, although with some simplifications, the geometry and material properties can be changed to represent working prototypes. This can be used to regress kinetic parameters on new materials once experimental data for these prototypes are available, and later use these information to optimize the operating conditions and geometrical and morphological aspects of the cell.

Nomenclature

Glossary

A^{des}	Pre–exponential factor of hydrogen desorption kinetics [s · m^2 · mol^{-1}]
a_m	Specific area for reaction m [m^{-1}]
$\boldsymbol{d}_i$	Diffusional driving force for species i []
D_{ij}	Binary diffusion coefficient for species i and j [m^2 · s]
E_j^{act}	Activation energy (j = a, c) [J · mol-1]
E_{des}	Activation energy of hydrogen desorption kinetics [J · mol^{-1}]
F	Faraday constant [C · mol^{-1}]
i_0	Amplitude of sinusoidal current density [A · m^{-2}]
i_{0j}	Exchange current per unit of TPB length (j = a, c) [A · m^{-1}]
$i_{0\,i}^{ref}$	Exchange current per unit of TPB length at the reference temperature (j = a, c) [A · m^{-1}]
i_j	Current density per unit of TPB length (j = a, c) [A · m^{-1}]
i_m	Local current density for reaction m [A · m^{-2}]
$\boldsymbol{j}_i$	Mass flux vector of species i [kg · m^{-2} · s^{-1}]
MW_i	Molecular weight of species i [kg · mol^{-1}]
N_i	Molar flux of species i [mol · m^{-2} · s^{-1}]
n_m	Number of electrons participating in reaction m
OCV	Open circuit voltage [V]
P	Pressure [Pa]
$P_{H_2}^*$	Reference pressure of hydrogen adsorption/desorption equilibrium [Pa]
p_i	Partial pressure of species i [Pa]
Q_{br}	Generation/consumption of matter in the porous matrix [kg · m^{-2} · s^{-2}]
R	Ideal gas constant [J · mol^{-1} · K^{-1}]
R_i	Production rate of species i [kg · m^{-3} · s^{-1}]
T	Temperature [K]
T_i^{ref}	Reference temperature for reaction kinetics (j = a, c) [K]
u	Velocity Field [m · s^{-1}]
V	Voltage [V]
V^0	Standard voltage [V]
V_0	Amplitude of sinusoidal voltage [V]
V_p	Electric potential of phase p (p = *el,a*; *el,c; io*)
w_i	Mass fraction of species i
y_i	Molar fraction of species i

Z	Impedance [$\Omega \cdot m^2$]
Z_0	Amplitude of impedance [$\Omega \cdot m^2$]
α_j	First transfer coefficient ($j = a, c$)
β_j	Second transfer coefficient ($j = a, c$)
Γ	Surface site density [$mol \cdot m^{-2}$]
γ_0	Sticking probability of hydrogen adsorption kinetics
ΔG_0^f	Change in molar Gibbs free energy of formation [$J \cdot mol^{-1}$]
ζ	Reaction order of oxygen in cathode kinetics
η_{cell}	Cell overpotential [V]
η_j	Activation overpotential ($j = a, c$) [V]
κ	Permeability [m^2]
λ_{TPB}	TPB length per unit volume [m^{-2}]
μ_i	Dynamic viscosity of species i [$kg \cdot m^{-1} \cdot s^{-1}$]
$\nu_{i,m}$	Stoichiometric coefficient of species i in reaction m
ρ	Gas density [$kg \cdot m^{-3}$]
σ_p	Conductivity of phase p (p = *el,a; el,c; io*) [$S \cdot m^{-1}$]
φ	Phase shift [rad]
ϕ^{la}	Porosity of layer *la* (*la = cc, ca, af, as*)
$\chi_p^{eff,la}$	Effective conductivity factor of phase p (p = *el,a; el,c; io*) in the layer *la* (*la = cc, ca, af, as*)
Ψ_{el}	Solid volume fraction of electronic phase *el* (*el = ela*, *elc*) after sintering
ω	Frequency [Hz]

Subscripts

el,a	Electron–conducting phase in the anode
el,c	Electron–conducting phase in the cathode
io	Ion–conducting phase
rev	Reversible

Superscripts

af	Anode functional layer
as	Anode supporting layer
ca	Cathode layer
cc	Current collector
ey	Electrolyte

Abbreviations

FPMFj	Free and Porous Media Flow module in the side j (j = a, c)
LSM	Strontium Stabilized Lanthanum Manganite

SIEC	Secondary Current Distribution module
SOFC	Solid Oxide Fuel Cells
TCSj	Transport of Concentrated Species module in the side j (j = a, c)
TPB	Three Phase Boundary
YSZ	Yttria Stabilized Zirconia

Bibliography

1. J. Larminie, A. Dicks, Fuel Cell Systems Explained, Wiley, New York, 2003.
2. S.C. Singhal, K. Kendall, High temperature solid oxide fuel cells: fundamentals, design and applications, Elsevier, Oxford, 2003.
3. S.C. Singhal, Advances in solid oxide fuel cell technology, Solid State Ionics. 135 (2000) 305–313.
4. Viswanathan, B. and M.A. Scibioh, Fuel cells: principles and applications. 2007, Hyderabad Boca Raton, FL: Universities Press; Distributed by CRC Press. x, 494 p.
5. Singhal, S.C., Solid oxide fuel cells for stationary, mobile, and military applications. Solid State Ionics, 2002. 152–153(0): p. 405-410.
6. R.J. Kee, H. Zhu, D.G. Goodwin, Solid-oxide fuel cells with hydrocarbon fuels, Proc. Combust. Inst. 30 (2005) 2379–2404.
7. Bove, R. and S. Ubertini, Modeling Solid Oxide Fuel Cells Methods, Procedures and Techniques, in Fuel Cells and Hydrogen Energy. 2008, Springer: Dordrecht. p. 1 online resource (404 p.).
8. K.N. Grew, W.K.S. Chiu, A review of modeling and simulation techniques across the length scales for the solid oxide fuel cell, J. Power Sources. 199 (2012) 1–13.
9. Basu, R.N., et al., Simplified processing of anode-supported thin film planar solid oxide fuel cells. Journal of the European Ceramic Society, 2005. 25(4): p. 463-471.
10. Brett, D.J.L., et al., Intermediate temperature solid oxide fuel cells. Chemical Society Reviews, 2008. 37(8): p. 1568-1578.
11. Fergus, J.W., Metallic interconnects for solid oxide fuel cells. Materials Science and Engineering: A, 2005. 397(1–2): p. 271-283.
12. S.B. Adler, Factors governing oxygen reduction in solid oxide fuel cell cathodes, Chem. Rev. 104 (2004) 4791–4843.
13. J. Gao, X. Liu, D. Peng, G. Meng, Electrochemical behavior of Ln0.6Sr0.4Co0.2Fe0.8O3−δ (Ln=Ce, Gd, Sm, Dy) materials used as cathode of ITSOFC, Catal. Today. 82 (2003) 207–211.
14. M.T. Colomer, B.C.H. Steele, J.A. Kilner, Structural and electrochemical properties of the Sr0.8Ce0.1Fe0.7Co0.3O3-δ perovskite as cathode material for ITSOFCs, Solid State Ionics. 147 (2002) 41–48.
15. Wiezell, K.; Gode, P.; Lindbergh, G. Steady-state and EIS investigations of hydrogen electrodes and membranes in polymer electrolyte fuel cells: I. Modeling. Journal of the Electrochemical Society, 2006, 153, A749-A758

16. Gamry Instruments. Basics of Electrochemical Impedance Spectroscopy." Application Note, www.gamry.com/App_Notes/Index.htm. 2006
17. Latham RA. Algorithm Development for Electrochemical Impedance Spectroscopy Diagnostics in PEM Fuel Cells. Thesis Submitted in Partial Fulfillment of the Requirements for the Degree of MASTER OF APPLIED SCIENCE in the department of Mechanical Engineering. BSME, Lake Superior State University, 2001.
18. Comsol Inc., Comsol Multiphysics user's guide, version 3.5, Burlington, MA, 2008.
19. L. Blum, W. a. Meulenberg, H. Nabielek, R. Steinberger-Wilckens, Worldwide SOFC technology overview and benchmark, Int. J. Appl. Ceram. Technol. 2 (2005) 482–492
20. B. Kenney, K. Karan, Engineering of microstructure and design of a planar porous composite SOFC cathode: A numerical analysis, Solid State Ionics. 178 (2007) 297–306.
21. M. Andersson, H. Paradis, J. Yuan, B. Sundén, Three dimensional modeling of an solid oxide fuel cell coupling charge transfer phenomena with transport processes and heat generation, Electrochim. Acta. 109 (2013) 881–893.
22. V.A.C. Haanappel, J. Mertens, D. Rutenbeck, C. Tropartz, W. Herzhof, D. Sebold, et al., Optimisation of processing and microstructural parameters of LSM cathodes to improve the electrochemical performance of anode-supported SOFCs, J. Power Sources. 141 (2005) 216–226.
23. D. Simwonis, H. Thülen, F.J. Dias, A. Naoumidis, D. Stöver, Properties of Ni/YSZ porous cermets for SOFC anode substrates prepared by tape casting and coat-mix process, J. Mater. Process. Technol. 92-93 (1999) 107–111.
24. J. Mertens, V.A.C. Haanappel, C. Wedershoven, H.-P. Buchkremer, Sintering behavior of (La,Sr)MnO3 type cathodes for planar anode-supported SOFCs, J. Fuel Cell Sci. Technol. 3 (2006) 415–421.
25. E.A. Mason, A.P. Malinauskas, Gas transport in porous media: the dusty-gas model, Elsevier, Amsterdam, 1983.
26. D. Arnošt, P. Schneider, Dynamic transport of multicomponent mixtures of gases in porous solids, Chem. Eng. J. Biochem. Eng. J. 57 (1995) 91–99.
27. R. Suwanwarangkul, E. Croiset, M.W. Fowler, P.L. Douglas, E. Entchev, M.A. Douglas, Performance comparison of Fick's, dusty-gas and Stefan–Maxwell models to predict the concentration overpotential of a SOFC anode, J. Power Sources. 122 (2003) 9–18.
28. M. Bertoldi, T. Zandonella, V.A.C. Haanappel, J. Mertens, J. Remmel, L.G.J. de Haart, Demonstration of a 4-Cells SOFC stack under different experimental conditions, J. Fuel Cell Sci. Technol. 5 (2008) 011004.
29. D.G. Goodwin, H. Zhu, A.M. Colclasure, R.J. Kee, Modeling electrochemical oxidation of hydrogen in Ni-YSZ pattern anodes, J. Electrochem. Soc. 156 (2009) B1004–B1021.

30. J. Mizusaki, H. Tagawa, T. Saito, K. Kamitani, T. Yamamura, K. Hirano, et al., Preparation of nickel pattern electrodes on YSZ and their electrochemical properties in H2-H2O atmospheres, J. Electrochem. Soc. 141 (1994) 2129–2134.
31. H. Zhu, R.J. Kee, Modeling distributed charge-transfer processes in SOFC membrane electrode assemblies, J. Electrochem. Soc. 155 (2008) B715–B729.
32. B. Todd, J.B. Young, Thermodynamic and transport properties of gases for use in solid oxide fuel cell modelling, J. Power Sources. 110 (2002) 186–200.
33. J.H. Nam, D.H. Jeon, A comprehensive micro-scale model for transport and reaction in intermediate temperature solid oxide fuel cells, Electrochim. Acta. 51 (2006) 3446–3460.
34. H. Zhu, R.J. Kee, V.M. Janardhanan, O. Deutschmann, D.G. Goodwin, Modeling elementary heterogeneous chemistry and electrochemistry in solid oxide fuel cells, J. Electrochem. Soc. 152 (2005) A2427–A2440.
35. M. Bertoldi, T. Zandonella, V.A.C. Haanappel, J. Mertens, J. Remmel, L.G.J. de Haart, Demonstration of a 4-Cells SOFC stack under different experimental conditions, J. Fuel Cell Sci. Technol. 5 (2008) 011004.
36. Bertei, A. Mathematical Modeling of Solid Oxide Fuel Cells. Ph.D. Thesis, University of Pisa, Pisa, Italy, 10 February 2014.
37. D. Simwonis, H. Thülen, F.J. Dias, A. Naoumidis, D. Stöver, Properties of Ni/YSZ porous cermets for SOFC anode substrates prepared by tape casting and coat-mix process, J. Mater. Process. Technol. 92-93 (1999) 107–111.
38. V.N. Nguyen, Q. Fang, U. Packbier, L. Blum, Long-term tests of a Jülich planar short stack with reversible solid oxide cells in both fuel cell and electrolysis modes, Int. J. Hydrog. Energy 38 (2013) 4281-4290
39. Costamagna P., Costa P., Antonucci V., Micro-modelling of solid oxide fuel cell electrodes, Electrochimica Acta 43 (1998) 375-394.
40. Kim J., Virkar A.V., Fung K.Z., Metha K., Singhal S.C., J. Electrochemical Soc. 146 (1999) 69-78.
41. J.P. Neidhardt, M. Henke, W.G. Bessler, Kinetic modeling of nickel oxidation is SOFC anodes, ECS Trans. 35 (2011) 1621–1629.
42. M. Andersson, J. Yuan, B. Sundén, SOFC modeling considering electrochemical reactions at the active three phase boundaries, Int. J. Heat Mass Transf. 55 (2012) 773–788.
43. A. Bieberle, L.P. Meier, L.J. Gauckler, The electrochemistry of Ni pattern anodes used as solid oxide fuel cell model electrodes, J. Electrochem. Soc. 148 (2001) A646–A656.
44. A. Leonide, Y. Apel, E. Ivers-Tiffée, SOFC modeling and parameter identification by means of impedance spectroscopy, ECS Trans. 19 (2009) 81–109.

45. V. Sonn, A. Leonide, E. Ivers-Tiffée, Combined deconvolution and CNLS fitting approach applied on the impedance response of technical Ni/8YSZ cermet electrodes, J. Electrochem. Soc. 155 (2008) B675–B679.
46. M. Vogler, H. Störmer, D. Gerthsen, A. Utz, A. Weber, E. Ivers-Tiffée, et al., Electrochemistry and mechanism of hydrogen oxidation at Ni/YSZ patterned anodes, in: P. Connor (Ed.), 9th Eur. SOFC Forum, Lucerne - Switzerland, 2010, 0994–09103.
47. L. Holzer, D. Wiedenmann, B. Münch, L. Keller, M. Prestat, P. Gasser, et al., The influence of constrictivity on the effective transport properties of porous layers in electrolysis and fuel cells, J. Mater. Sci. 48 (2013) 2934–2952.
48. M.B. Pomfret, J. Marda, G.S. Jackson, B.W. Eichhorn, A.M. Dean, R.A. Walker, Hydrocarbon fuels in solid oxide fuel cells: in situ Raman studies of graphite formation and oxidation, J. Phys. Chem. C 112 (2008) 5232-5240
49. X. Lu, P.W. Faguy, M. Liu, in situ potential-dependent FTIR emission spectroscopy: a novel probe for high temperature fuel cell interfaces, J. Electrochem. Soc. 149 (2002) A1293-1298
50. N.Wagner, W.Schnurnberger, B.Müller, M.Lang, Electrochemical impedance spectra of solid-oxide fuel cells and polymer membrane fuel cells, Electrochimica Acta 43 (1998) 3785-3793